Targeted analysis of chondrocyte central metabolites in response to cyclical compression and shear deformations

[1]Erik P. Myers, [1]Aurora Gallagher, [1]Avery Welfley, [1]Samuel Battles, [1]Aidan Gregory, [1]Priyanka Brahmachary, [2]Mark Greenwood, and [1,3]Ronald K. June

Affiliations

[1]Department of Mechanical & Industrial Engineering, Montana State University, Bozeman MT.

[2]Department of Mathematical Sciences, Montana State University, Bozeman MT.

[3]Department of Microbiology & Cell Biology, Montana State University, Bozeman MT.

*Corresponding Author:

Ronald K. June, Ph.D.

Department of Mechanical & Industrial Engineering, Montana State University

PO Box 173800, Bozeman, MT 59717-3800 | Phone: (406) 994-5941; Fax: (406) 994-6292; E-mail: rjune@montana.edu

Abstract

Osteoarthritis results in deterioration of articular cartilage, the soft tissue covering articulating surfaces of bones in joints like the knee and hip. Prior studies show that cyclical mechanical stimulation of articular cartilage results in synthesis of cartilage matrix, suggesting that therapeutic mechanical stimulation might be beneficial for cartilage repair in osteoarthritis. Several prior studies identify ion channels and cytoskeletal molecules as components of chondrocyte mechanotransduction. The pathways of central metabolism, glycolysis, the pentose phosphate pathway, and the tricarboxylic acid cycle, are necessary for producing non-essential amino acids that are needed for synthesizing matrix proteins for cartilage repair. However, it is currently unknown if and how levels of central metabolites change with applied mechanical stimulation of chondrocytes. Here, we show that applied cyclical shear and compressive deformations drive changes in multiple central metabolites. These results add to a rich picture of chondrocyte mechanotransduction including calcium signaling, ion channels, integrins, and cytoskeletal components. By finding compression- and shear-induced changes in central metabolites, these data support the potential for therapeutic mechanotransduction toward cartilage repair. Future studies may build on these results to understand the relationships between mechanical stimulation and chondrocyte central metabolism.

Keywords

cartilage; chondrocyte; mechanotransduction; osteoarthritis; metabolism

Introduction

Articular cartilage is the soft tissue lining diarthrodial joints like the knee and hip. This tissue contains a single cell type—the articular chondrocyte—and is subjected to cyclical loads during daily activities such as walking. These loads cause tissue-level deformations that result in mechanical stimulation of articular chondrocytes. Tissue-level deformations include tension, compression, and shear-based on *in vivo* measurements (Chan et al. 2016).

A key feature of the most common joint disease, osteoarthritis (OA), is the deterioration of articular cartilage (Tonge et al. 2014). This deterioration results in alterations of both the extracellular and pericellular cartilage matrices, with concomitant changes in various cartilage mechanical properties. For example, after joint injury, there are significant decreases in the indentation modulus of the mouse pericellular matrix after just 3 days with a reduction of ~50% after 1 month (Chery et al. 2020). In contrast, exercise typically results in improved cartilage health. Patients with a history of marathon running had ~25% thicker cartilage than age-matched controls (Mosher et al. 2010).

Early observations show that cyclical mechanical stimulation of cartilage and chondrocytes results in production of matrix molecules (Mauck et al. 2006; Sah et al. 1989) through chondrocyte mechanotransduction. This shows the potential for mechanical stimulation to drive therapeutic production of matrix for cartilage repair. While several ion channels (Ely et al. 2025) and various cytoskeletal components (Haudenschild et al. 2011; Ohashi et al. 2006) have been implicated in chondrocyte mechanotransduction, many questions remain regarding the specific cascade of signals that results in increased matrix production.

68 Central metabolism (*i.e.* energy metabolism) is a network of enzymes and small
69 molecule intermediates called metabolites used by cells to harvest carbon and energy to
70 support cellular function. Substrates include glucose and glutamine, which can be
71 metabolized to produce non-essential amino acids. Functioning central metabolism,
72 including both glycolysis and cellular respiration, involves oxygen consumption and is
73 essential for producing the non-essential amino acids required for cartilage regeneration.
74 For example, non-essential amino acids make up 83.1, 71.4, and 74.5% of the primary
75 sequences for the key cartilage matrix proteins encoded by COL2A1, COL6A1, and
76 ACAN (types II and VI collagen and aggrecan).

77 We hypothesized that mechanical stimulation would alter the production of central
78 metabolites in articular chondrocytes. Toward this goal, we harvested articular
79 chondrocytes, expanded them in monolayer culture, and then encapsulated them in
80 physiologically stiff agarose (Jutila et al. 2015; Zignego et al. 2014). Embedded
81 chondrocytes were then stimulated with cyclical shear and compressive strains at
82 physiological levels. Immediately after mechanical stimulation, metabolites were
83 extracted. Levels of central metabolites were then quantified using targeted metabolomic
84 profiling. We found changes in levels of several metabolites demonstrating that
85 mechanical stimulation affects chondrocyte central metabolism. Futures studies can build
86 on these results to further understand how mechanical stimuli influence chondrocyte
87 metabolism to maintain cartilage and improve repair during disease.

88 **Methods**

89 Chondrocyte harvest and culture

90 To assess central metabolism in chondrocyte mechanotransduction, chondrocytes
91 were isolated from cartilage using established methods (Zignego et al. 2015; Zignego et
92 al. 2014). Primary Human Chondrocytes (PHCs) were obtained from discarded tissue
93 from Stage-IV osteoarthritis patients (n=5 male and n=5 female) undergoing total joint
94 replacement under IRB approval. Bovine chondrocytes (BCs, n=5) were harvested from
95 knee joints of 18–22-month-old cattle obtained from a local abattoir. Articular cartilage
96 was digested with Type I Collagenase (2 mg/mL in DMEM with penicillin and
97 streptomycin, Gibco, Waltham, MA, USA) for 14 h at 37 ºC. Isolated chondrocytes were
98 cultured in phenol-red-free Dulbecco's Modified Eagle's medium (DMEM, Gibco,
99 Waltham, MA, USA) supplemented with Fetal Bovine Serum (FBS, 10% v/v, Bio-Techne,
100 Minneapolis, MN, USA), penicillin (10,000 I.U./mL), and streptomycin (10,000 µg/mL,
101 Sigma, St. Louis, MO, USA) in 5% CO2 at 37 ºC. First passage cells were used for
102 experiments.

103 To provide a three-dimensional environment in the range of physiological stiffness,
104 chondrocytes were encapsulated in high-stiffness agarose (Jutila et al. 2015). After
105 trypsinization, cells were washed with 1X PBS and resuspended in DMEM (without
106 phenol red) and mixed with low melting temperature agarose (Sigma Aldrich) at a final
107 concentration of 4.5% wt/vol with ~500,000 cells/gel and allowed to solidify for 10 min.
108 Hydrogels were cast in a cylindrical aluminum mold to have a nominal diameter of 0.5"
109 and a height of 0.25" following a previously established protocol (Jutila et al. 2015). In this
110 system, chondrocyte viability was previously found to be >90% (Zignego et al. 2014).

111 Agarose gels were placed in a 24-well tissue culture plates (Falcon) with 2 mL custom
112 DMEM media containing 4.5g/L glucose, 2 mM L-glutamine,110mg/L sodium pyruvate,
113 10% FBS, and 1% PenStrep and cultured overnight in 5% CO_2 at 37ºC. Prior to loading
114 media was replaced with PBS for 1 hr and incubated in 5% CO_2 at 37ºC.

115

116 Mechanical Stimulation

117 To evaluate the effects of physiological loading on chondrocyte central metabolism,
118 agarose-embedded chondrocytes were subjected to mechanical stimuli. Stimuli included
119 applied cyclical shear and compressive strains in a tissue culture environment. A total of
120 N=10 PHCs (n=5 male and n=5 female) and N=5 BC samples were used.

121 Chondrocyte-embedded agarose constructs from each bovine or human donor were
122 randomized into five experimental groups: Unloaded controls (U), 15 minutes of cyclical
123 compressive strain (15C), 15 minutes of cyclical shear strain (15S), 30 minutes of cyclical
124 compressive strain (30C), and 30 minutes of cyclical shear strain (30S). For both
125 compressive and shear stimulation, mean strains were 5% with an amplitude of 2.5%.
126 Each experiment was performed at 1.1Hz with 5% preload applied for 15 minutes to allow
127 for stress relaxation. Mechanical stimulation of samples from each donor was completed
128 over the course of a single day. On instances where multiple donors were available on
129 the same day, simultaneous loading for each group across all available donors was
130 performed.

131 For each loading group, the hydrogel was removed from PBS, placed within the
132 polysulfone sample cup, and resubmerged in fresh PBS to prevent drying during loading

133 (Figure 1). The bioreactor was then placed inside the trigas incubator and powered on to
134 provide mechanical stimulation within a tissue culture environment. In the case of an
135 uneven number of hydrogels, an agarose hydrogel containing no cells was used to
136 balance the load from the hydrogels on the plunger plate.

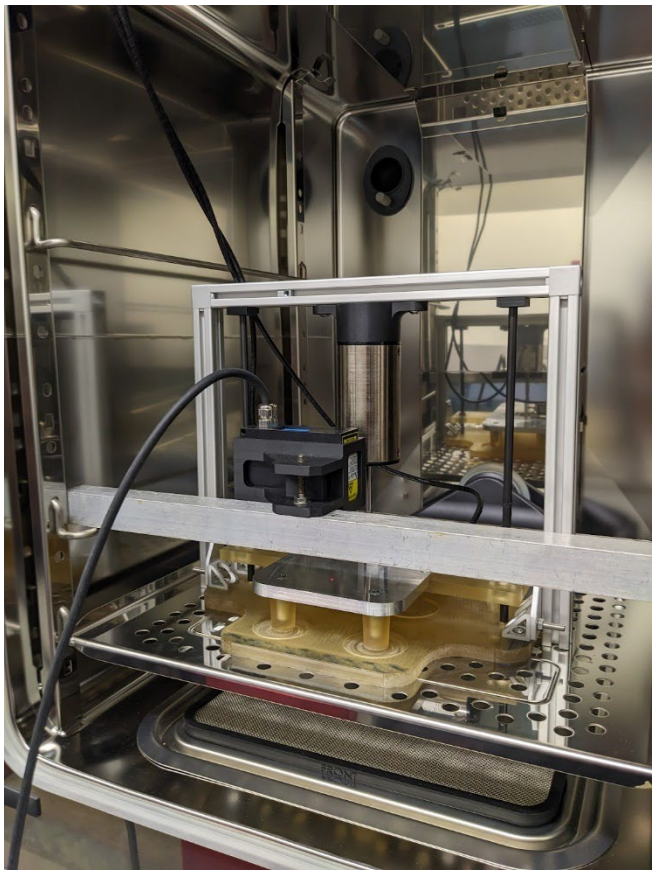

137

138 *Figure 1: Chondrocyte bioreactor inside a trigas incubator with laser displacement*
139 *sensor suspended overhead. During normal experimentation, the sensor is absent from*
140 *the incubator.*

141 Immediately after mechanical stimulation, hydrogels were removed from the
142 bioreactor and bisected using a sterile scalpel. One-half of the sample was used for
143 oxygen measurement and the other half was used for targeted metabolomic analysis.

Oxygen Measurement and Metabolite Extraction

An oxygen measurement system (OX-10, Unisense, Aarhus, Denmark) was used to quantify oxygen tension immediately after mechanical stimulation. Probes were calibrated to 0% O_2 tension using a nitrogen sparged water bath and 100% O_2 tension using an atmospheric air sparged water bath. 2-point calibration curves were then used to quantify oxygen saturation readings from each bisected sample. The oxygen probe was inserted into the hydrogel and oxygen readings were measured for 1 minute, with the minimum oxygen tension during the measurement recorded for each sample (Figure 2).

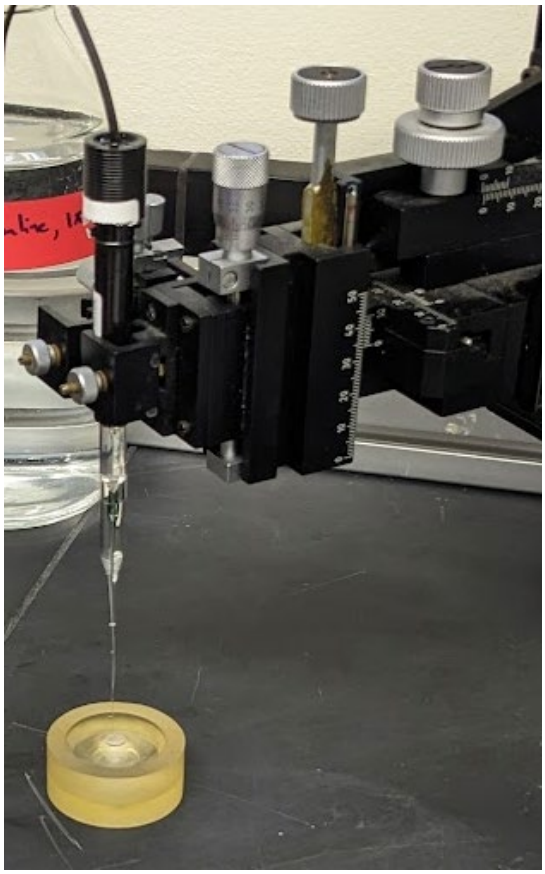

Figure 2: Oxygen probe needle embedded within an agarose hydrogel. The probe was retracted after each reading and used to collect a pre and post reading atmospheric baseline.

156 The other half of the hydrogel which was not probed for oxygen readings was
157 immediately wrapped in autoclaved aluminum foil and flash-frozen in liquid nitrogen to
158 preserve current metabolite levels after mechanical stimulation. After freezing for 1-2
159 minutes, the gel was extracted and crushed using a sterile aluminum rod. The pulverized
160 hydrogel was then placed in a 2.5mL Eppendorf tube and allowed to freeze in -80°C
161 overnight. This process was completed for all hydrogels for all experimental groups. After
162 freezing for at least 12 hours, the crushed gels were removed from the freezer and
163 homogenized into a powder using a Cryomill (Verder Scientific, Haan, Germany).
164 Following Cryo-milling, the powder was suspended in extraction buffer (70:30:1%
165 Methanol:Acetone:formic acid). Formic acid facilitated metabolite release from the
166 homogenized agarose (Supplemental Material B). Each hydrogel was extracted with 5mL
167 of extraction buffer at -80°C overnight. The following morning, samples were centrifuged
168 (4,000 rpm, 10 minutes), and the supernatant was extracted and dried down using a
169 vacuum centrifuge at 45°C (Eppendorf, Hamburg, Germany) until only the dried pellet of
170 concentrated metabolites remained. These metabolite pellets were then resuspended in
171 50μL 50:50 HPLC water:acetonitrile and sent for mass spectrometry analysis.

172 Mass spectrometry analysis of mechanically stimulated constructs

173 After metabolite extraction, levels of central metabolites were quantified using LC-MS
174 and a previously established protocol (Brahmachary et al. 2023) (Liquid Chromatography-
175 Mass Spectrometry, C18 Column, Agilent 6538 Q-TOF). Quality control included analysis
176 of blank samples of 50:50 HPLC Water:Acetonitrile every ten samples. For quantification,
177 analytical standards containing 18 key central carbon metabolites were included within
178 the run at concentrations of 100, 50, 10, 5, 2, and 1μg/mL. To quantify individual

179 metabolite concentrations, calibration curves were constructed based on the known
180 standard concentration and the measured intensity (Supplemental Material C). A pool was
181 created for each loading group and was assembled from 5 randomly chosen 10μL
182 samples from each group to aid in fragmentation identification of each standard
183 metabolite in the sample. After the mass spectrometry analysis was completed, sample
184 data were converted from intensity peaks into concentration values and exported for
185 statistical analysis and visualization.

186 Statistical analysis of metabolites

187 Once the data had been trimmed, the remaining three male human, three female
188 human, and five bovine donors could be combined for a total of 65 samples and analyzed
189 on a per-metabolite basis. A total of 18 standard metabolites were used for mass
190 spectrometry calibration; Two different forms of NADH as well as HSCoA were not
191 detected due to low measured experimental values, leaving a total of 15 central
192 metabolites for comparison (Supplemental Material C). Metabolites and their pathways
193 within central carbon metabolism were identified and calibration ability was recorded for
194 all 18 metabolites (Table 1).

195 *Table 1: Individual metabolites paired with their common pathway name and branch*
196 *association when used in central carbon metabolism. Calibration capability and*
197 *statistical significance is also reported as checks or X's.*

Metabolite Name (Pathway Name)	Pathway Branch Involvement	Calibrated using Standards	Statistically Significant betw. groups	Significant Groups

#1 Oxaloacetic Acid (Oxaloacetate)	TCA Cycle	✅	❌	
#2 Fumaric Acid (Fumarate)	TCA Cycle	✅	❌	
#3 Phosphoenolpyruvic Acid (PEP)	Glycolysis	✅	❌	
#4 Malic Acid (Malate)	TCA Cycle	✅	✅	U-15C, U-30C, U-30S
#5 2-Oxoglutaric Acid (α-ketoglutarate)	TCA Cycle	✅	❌	
#6 6-p-gluconate	PPP	✅	❌	
#7 Citric Acid (Citrate)	TCA Cycle	✅	❌	
#8 Sedoheptulose-7-phosphate	PPP	✅	❌	
#9 Succinic Acid (Succinate)	TCA Cycle	✅	✅	U-30S, 15S-30S
#10 Fructose-6-phosphate	Glycolysis	✅	❌	

#11 Glutamic Acid (Glutamine)	TCA Cycle	✅	❌	
#12 Lactic Acid (Lactate)	Glycolysis	✅	✅	U-30S
#13 Glutamine	TCA Cycle	✅	✅	U-15C, U-30C, U-15S, U-30S
#14 Fructose / Glucose (Glucose)	Glycolysis	✅	✅	U-30C, U-30S
#15 Pyruvic Acid (Pyruvate)	Glycolysis	✅	✅	U-15C, U-30C, U-15S, U-30S
#16 $NADH_1$ (NADH)	All	❌	❌	
#17 HSCoA	TCA Cycle	❌	❌	
#18 $NADH_2$ (NADH)	All	❌	❌	

For each of the detectable 15 metabolites, statistical analysis was performed using Graphpad Prism. Outlier identification was performed using the ROUT method. One-way ANOVA was performed to test for differences in mean concentrations between the experimental groups. Additional pairwise comparisons were performed using Tukey's HSD for multiple testing correction. T-tests were used to compare metabolite levels between chondrocytes from male and female donors using the Holm-Sidak correction for

205 multiple testing between experimental groups. Metabolites with significant differences are
206 visualized using violin plots. Statistical significance between group concentrations is
207 reported using the asterisk system (*: $p<0.05$ | **: $p<0.01$ | ***: $p<0.001$ | ****: $p<0.0001$).
208 All other metabolites without detectable group differences are shown in violin plots in
209 Supplemental Material D.

210 **Results**

211 Oxygen Concentration

212 While oxygen readings were performed for each hydrogel that was loaded during the
213 experimentation process, statistical analysis of the oxygen readings revealed no
214 significant differences in oxygen tension regardless of loading condition. This is likely
215 because there was not sufficient time for chondrocytes to utilize measurable oxygen
216 during the short time span of the mechanical stimulation.

217 Targeted Metabolomics

218 Toward understanding how mechanical stimuli affects chondrocyte central metabolite
219 levels, we performed targeted metabolomic profiling after cyclical shear and compressive
220 stimulation. Six of the fifteen measured metabolites resulted in at least one significant
221 between-group difference. Of these six, three are related to glycolysis and three are
222 related to the TCA cycle. Five out of six metabolites showing significant differences and
223 also decreases in quantity in the mechanically stimulated groups suggesting that
224 mechanical stimulation either decreased production or increased consumption of these
225 metabolites. For the human OA donors, there were no detected differences in any
226 measured metabolite levels between male and female donors (n=5 each).

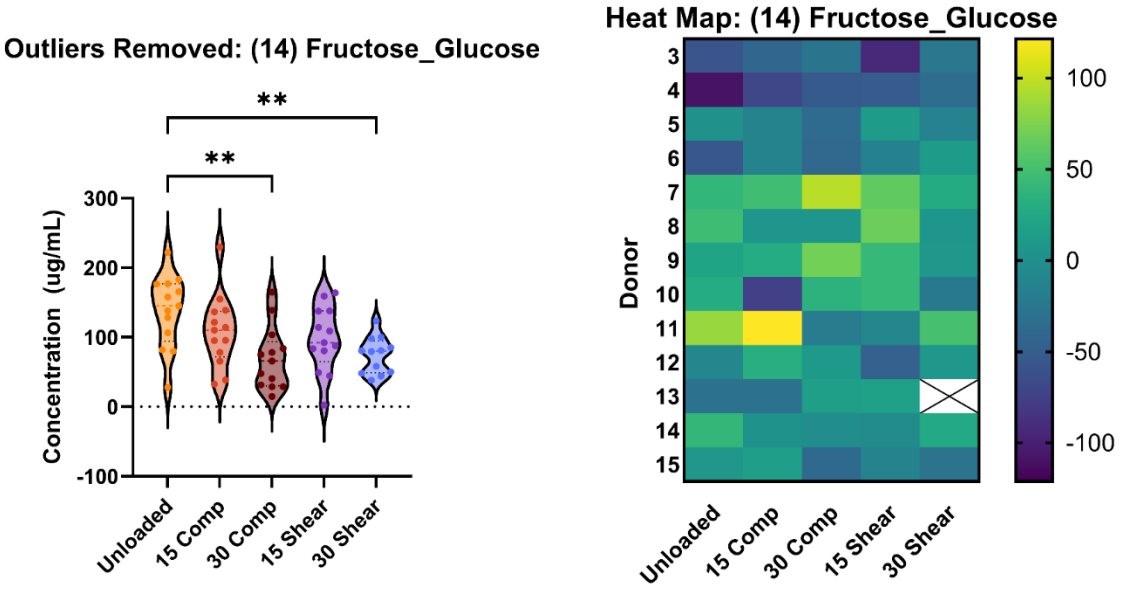

Figure 3: Concentration values for glucose decreased significantly when hydrogels were exposed to loading for 30 minutes. Note that because the cells are cultured and suspended in high-concentration glucose during expansion and embedding that glucose levels are naturally orders of magnitude above other metabolites.

Glucose, the input to glycolysis, decreased after both 30 minutes of cyclical compression and shear compared to unloaded controls (Figure 3).

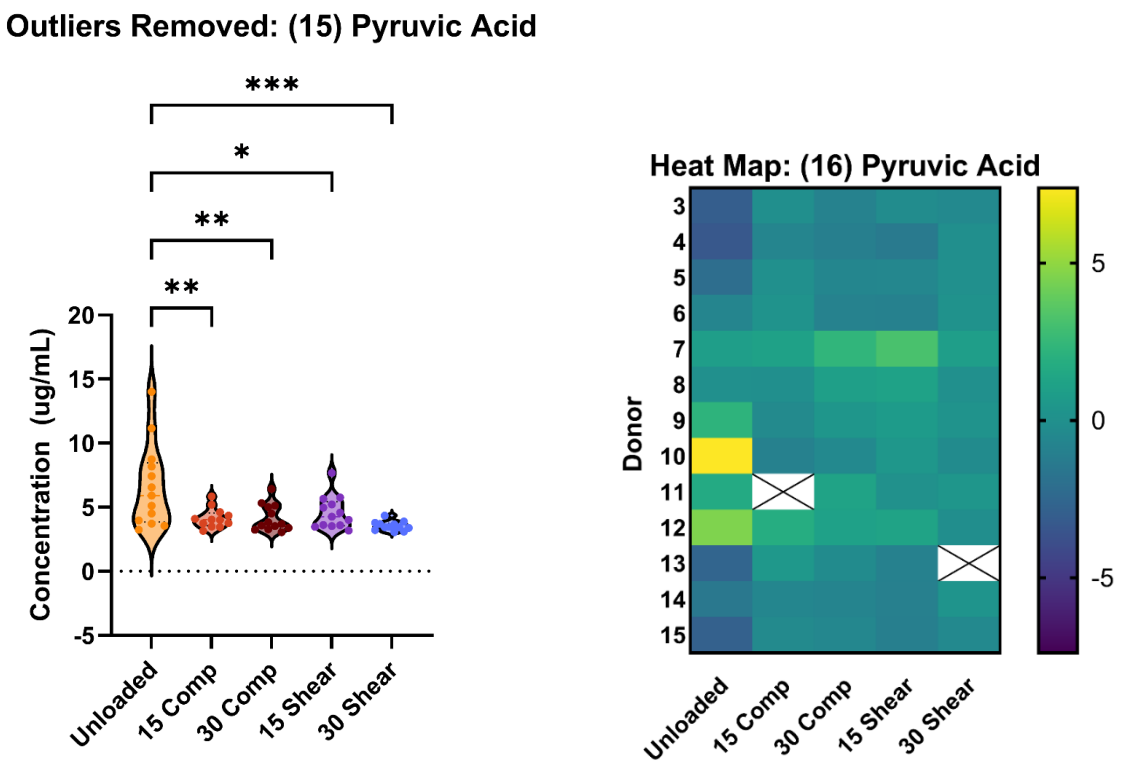

Figure 4: pyruvic acid levels showed a dramatic decrease in all groups when compared to the unloaded control. Note that the unloaded control group exhibited right-skewedness, while the other loaded groups were relatively uniform.

The output of glycolysis, pyruvate, decreased in response to both 15 and 30 minutes of both shear and compressive stimulation (Figure 4).

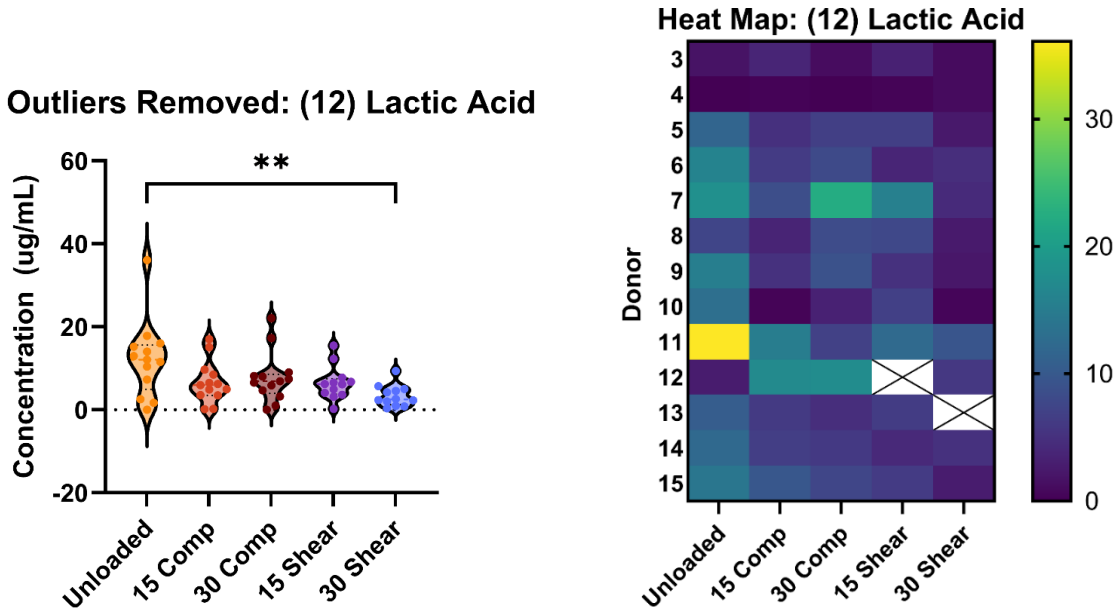

Figure 5: Lactic acid levels were decreased across all samples, but only the 30-minute shear group showed a statistically significant difference.

Pyruvate can be converted to lactate, and lactate decreased after 30 minutes of shear stimulation (Figure 5). These results indicate that there was substantial consumption of glycolytic metabolites in response to both applied shear and compression for chondrocytes.

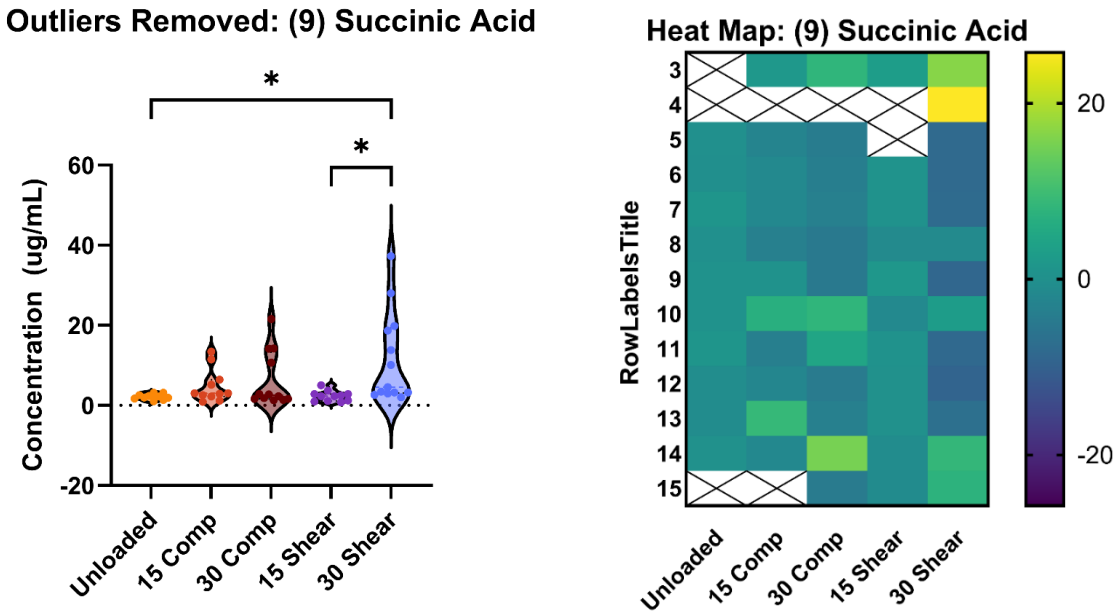

Figure 6: Succinic acid shows up-concentration in only the 30-minute shear group when compared to the unloaded or 15-minute shear group. It should be noted that both compression groups and the 30S group showed a right-skewed distribution of concentration when compared to the unloaded and 15S groups.

Within the TCA cycle, succinate increased after 30 minutes of shear stimulation compared to both 15 minutes of shear and unloaded controls (Figure 6).

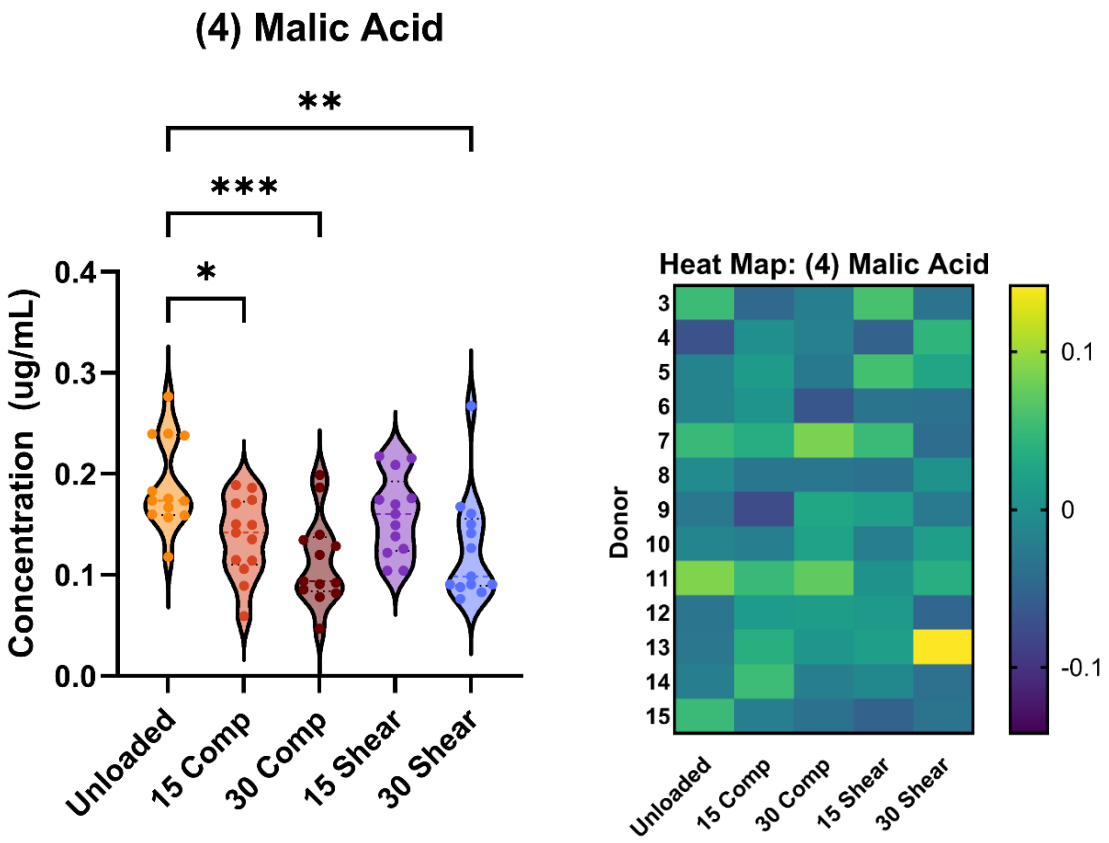

Figure 7: Malic Acid showed a decrease in concentration between the unloaded control group and the 15min & 30 min compression groups that was significantly different. The control also showed significant difference when compared to the 30min shear group.

Malate levels decreased after 15 and 30 minutes of compression as well as 30 minutes of shear stimulation (Figure 7).

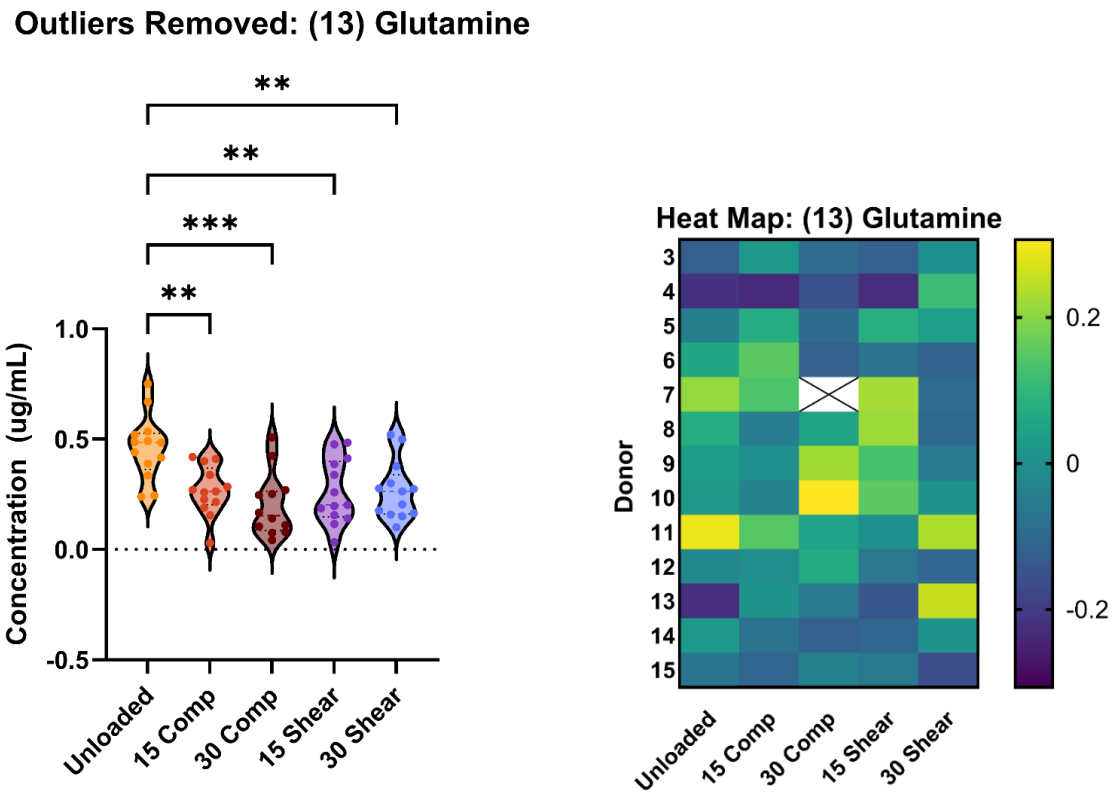

Figure 8: Concentration values for all loading durations and orientations showed a decrease in glutamine concentration relative to the control values that was significantly different.

Glutamine can provide carbon to the TCA cycle, and glutamine levels decreased for both 15 and 30 minutes of compression and shear compared to unloaded controls (Figure 8). These data indicate that cyclical shear and compression induced substantial TCA activity in articular chondrocytes.

Discussion

This study explored how cyclical mechanical stimulation influences chondrocyte metabolism using targeted metabolomic profiling of molecules from glycolysis, the

277 pentose-phosphate pathway, and TCA cycle. Variation in key metabolites reveals
278 details into how chondrocyte activity responds to cyclical shear and compressive stimuli.
279 Importantly, the complexity of these larger biochemical networks limits the
280 interpretability of metabolite dysregulation as a change in abundance could result from
281 changes in either production and/or consumption of any given metabolite (Doran et al.
282 2024).

283 Glycolytic metabolites (glucose, pyruvate, and lactate) were substantially
284 decreased in mechanically stimulated samples compared to unloaded controls, which
285 may be a result of decreased production, increased consumption, or a combination
286 thereof. This may indicate a shift toward a glycolytic, Warburg-like profile often seen in
287 pathological conditions (Jiang et al. 2023) or increased fueling of the TCA cycle to
288 promote production of non-essential amino acids for production of matrix proteins.

289 Additionally, glutamine—a primary carbon source for the TCA cycle—was
290 reduced in all mechanically stimulated groups compared to unloaded controls, indicating
291 dysregulated glutamine metabolism as a result of mechanical stimulation. Succinate
292 levels increased under both shear and compressive loading which may be linked with
293 downstream redox signaling or mitochondrial stress, as supported by findings in
294 osteoarthritic bone tissues (Shodiev et al. 2024). Alternatively, this altered TCA activity
295 may support production of key non-essential amino acids for matrix production. These
296 results suggest that mechanical loading affects metabolic activity in chondrocytes, likely
297 through increased energy demand that may be associated with cell stress and/or
298 production of non-essential amino acids for protein synthesis.

299

300 Beyond this system, our findings may have broader implications for cyclical
301 loading in osteoarthritis progression. The effect of mechanotransduction on central
302 metabolism and signaling is increasingly recognized in all joint tissues (Zhao et al.
303 2020). These results support the idea that metabolism is not a passive outcome of cell
304 function, rather a key response to mechanical signals. This is an emerging paradigm
305 with great therapeutic potential as increased understanding might lead to therapeutic
306 exercise interventions that use mechanical stimuli to direct chondrocyte metabolism
307 toward increased production of non-essential amino acids for protein production and
308 maintenance of the extracellular matrix.

309 A primary limitation of this study is that these targeted metabolomic profiles only
310 provide a static snapshot of metabolite levels at 15-minute time intervals. For oxygen
311 consumption, it is likely that measuring oxygen consumption immediately after loading
312 does not provide sufficient time for chondrocytes to appreciably consume oxygen, and
313 later timepoints might provide additional insights. Furthermore, without advanced
314 stoichiometric modeling, we cannot determine whether changes reflect altered
315 production or consumption (flux) of individual metabolites.

316 Future work should incorporate improved temporal resolution potentially with live
317 cell imaging, functional assays, stoichiometric modeling, and isotope tracing to better
318 resolve metabolic flux and pathway dynamics. These methods would help quantify
319 nutrient utilization and identify specific biochemical reactions altered by mechanical
320 stimuli. Given the small sample size (n=5 each) of male and female donors, future

321 studies should also explore potential sex differences, hormonal influences, and
322 mitochondrial regulation in more detail. These findings could ultimately guide tissue
323 engineering approaches and personalized interventions for OA by identifying optimal
324 mechanical loading parameters that support metabolic-based repair and maintenance of
325 articular cartilage.

326 These mechanically induced metabolic changes may serve as both a mechanism
327 of adaptation and a contributor to degeneration, depending on cellular context and load
328 magnitude. In healthy tissue, enhanced mitochondrial metabolism under physiological
329 loading supports ECM synthesis and redox homeostasis, facilitating tissue maintenance
330 and adaptation (Coleman et al. 2016). However, excessive loading can shift the
331 metabolic profile toward upregulated glycolysis,and impaired mitochondrial respiration.
332 This metabolic reprogramming can cause an accumulation of metabolic intermediates
333 and increased production of reactive oxygen species, which can activate inflammatory
334 cascades and drive the expression of inflammatory cytokines (Huang et al. 2023; Tan
335 et al. 2022). Overall, these data suggest that mechanical stimuli drive changes in central
336 metabolism in primary chondrocytes with potential implications for production of non-
337 essential amino acids needed for cartilage homeostasis. Additionally, results further
338 highlight mechanical signals as an active mediator of metabolism in chondrocytes and
339 regulation may prove a promising target for modulating tissue health in both normal and
340 disease states.

Acknowledgements

The authors are grateful for the assistance of Dr. Donald Smith for mass spectrometry assistance. This study was supported by the National Institutes of Health under Award Numbers R01AR073964 and R01AR081489 (RKJ) and the National Science Foundation under Award Number CMMI 1554708 (RKJ). Funding for the Montana State Mass Spectrometry Facility (RRID: SCR_012482) used in this publication was made possible in part by the MJ Murdock Charitable Trust, the National Institute of General Medical Sciences of the National Institutes of Health under Award Numbers P20GM103474 and S10OD28650, and the MSU Office of Research and Economic Development.

Conflict of Interest

Drs. June and Brahmachary are co-founders of OpenBioWorks. Dr. June also owns stock in Beartooth Biotech. These companies were not involved in this study.

Supplemental Material

A: Bioreactor Design and Drawings

Bioreactor design was based loosely on the format of modern 3-d printers like the Ender 3 Pro. In this design, a gantry suspends actuated components above a working volume. Primary design materials were selected to be both 6061 hot extruded/rolled aluminum, and polysulfone. These materials are corrosion resistant, relatively easy to machine, are safe to autoclave, and readily available (McMaster-Carr). CAD work was performed primarily in SolidWorks Design Suite. Post-Processing CAM G-code was produced using Fusion-360 for each sub-assembly component exported from

SolidWorks. Milling work was done primarily using a SuperMax-YCM 30 CNC endmill and Fagor 8025 controller. Lathe work was performed using an Enco 1236 metal lathe. All components which were not readily available for purchase were designed and manufactured in-house. The final rendered design is shown below.

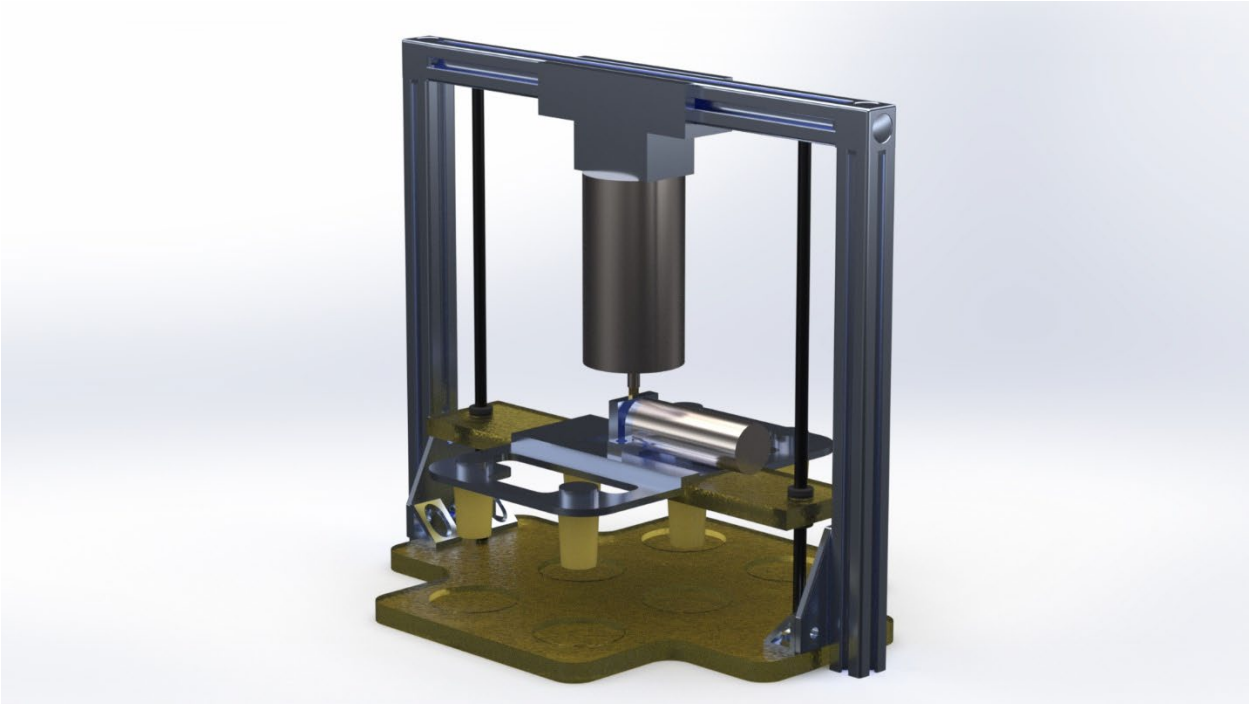

Render of fully assembled machine, showing differences in component material and assembly orientation.

Off-the-shelf components were used when available. Drawings for each individual custom component are listed below.

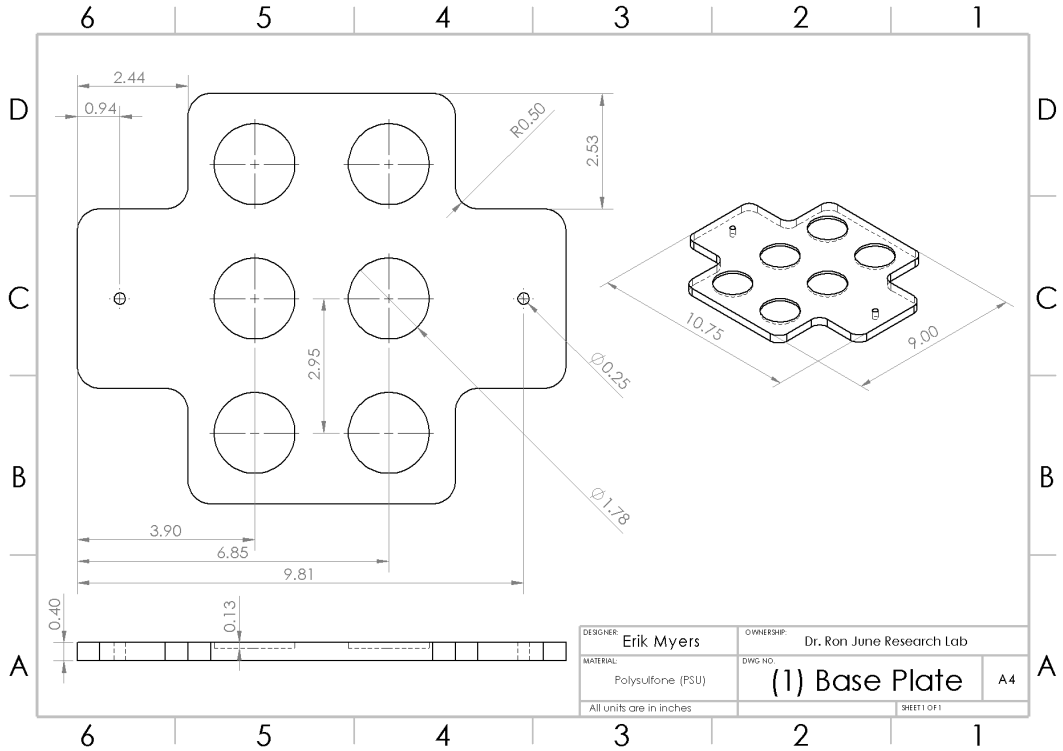
2.44
0.94
R0.50
2.53
2.95
Ø0.25
Ø1.78
3.90
6.85
9.81
0.40
0.13
10.75
9.00
DESIGNER: Erik Myers
OWNERSHIP: Dr. Ron June Research Lab
MATERIAL: Polysulfone (PSU)
DWG NO. (1) Base Plate
A4
All units are in inches
SHEET 1 OF 1

371

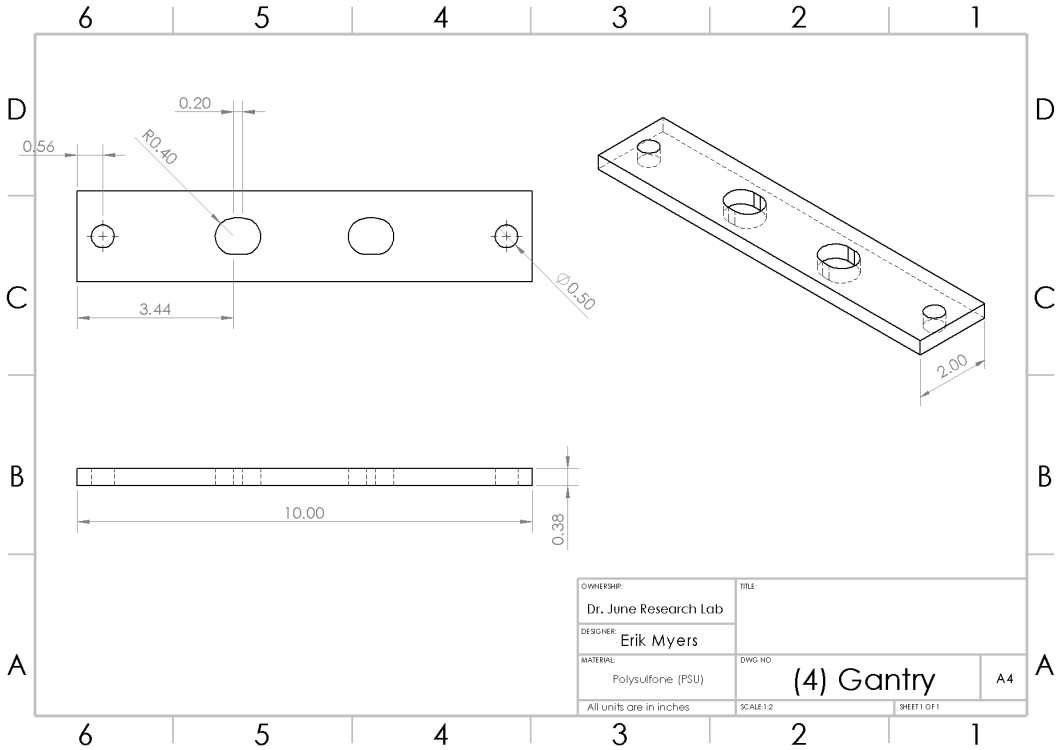
0.20
0.56
R0.40
Ø0.50
3.44
2.00
10.00
0.38
OWNERSHIP: Dr. June Research Lab
TITLE:
DESIGNER: Erik Myers
MATERIAL: Polysulfone (PSU)
DWG NO. (4) Gantry
A4
All units are in inches
SCALE:1:2
SHEET 1 OF 1

372

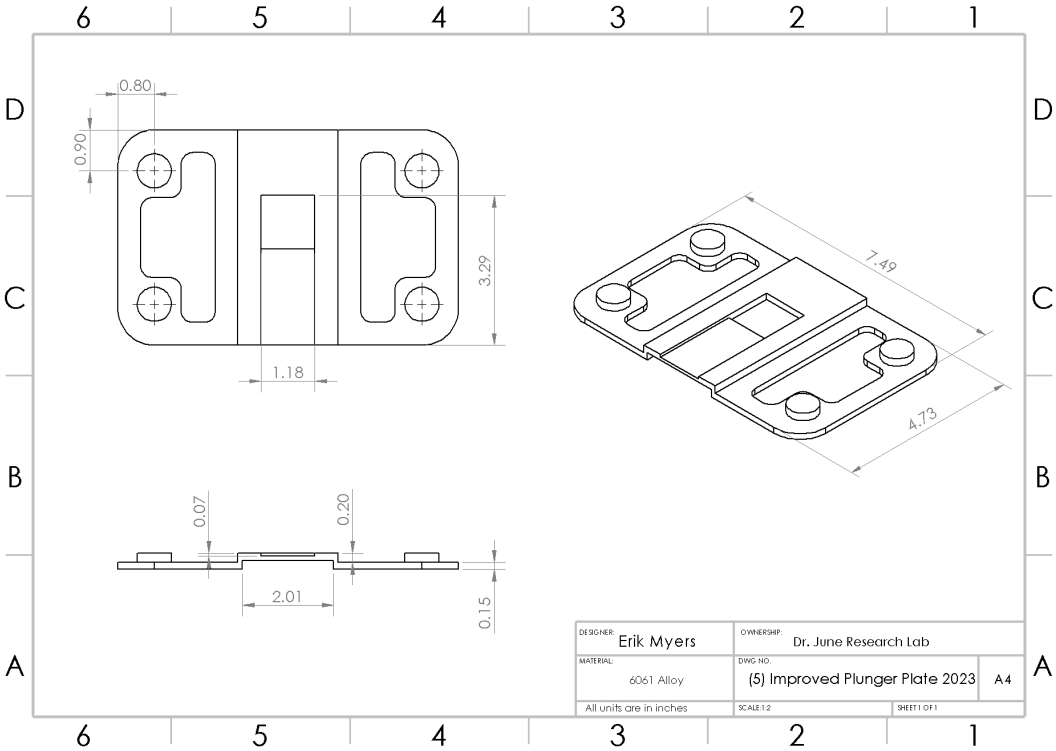
0.80
0.90
3.29
1.18
7.49
4.73
0.07
0.20
2.01
0.15
DESIGNER: Erik Myers
OWNERSHIP: Dr. June Research Lab
MATERIAL: 6061 Alloy
DWG NO. (5) Improved Plunger Plate 2023
A4
All units are in inches
SCALE:1:2
SHEET 1 OF 1

373

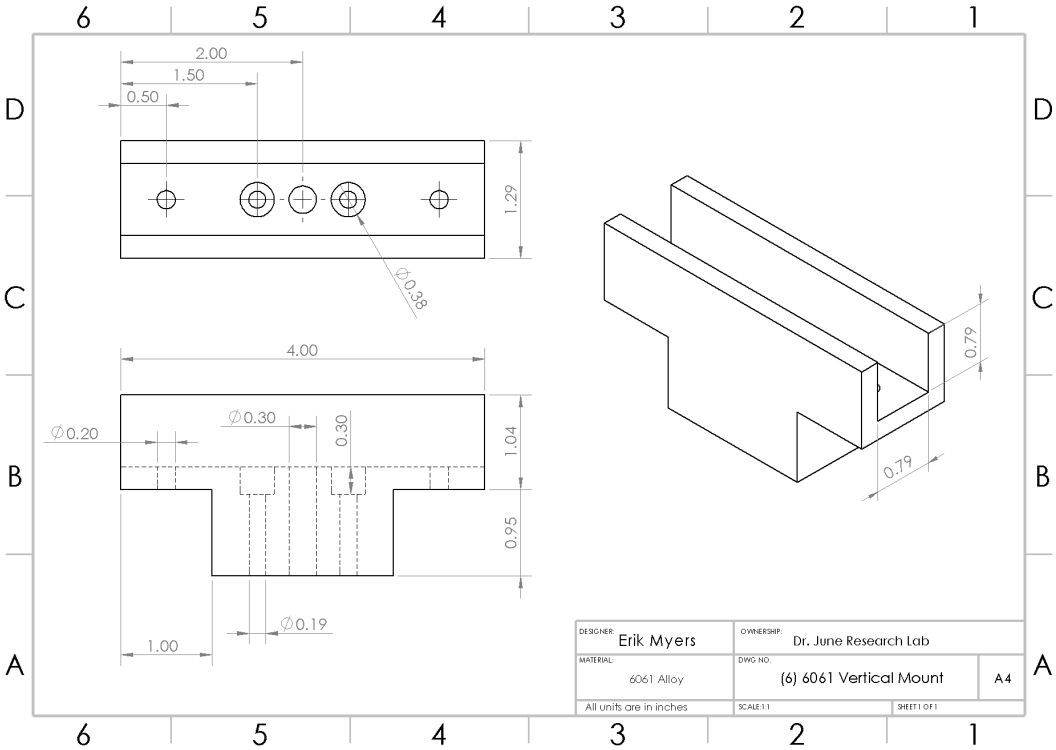
2.00
1.50
0.50
1.29
∅0.38
4.00
∅0.20
∅0.30
0.30
1.04
0.95
∅0.19
1.00
0.79
0.79
DESIGNER: Erik Myers
OWNERSHIP: Dr. June Research Lab
MATERIAL: 6061 Alloy
DWG NO. (6) 6061 Vertical Mount
A4
All units are in inches
SCALE:1:1
SHEET 1 OF 1

374

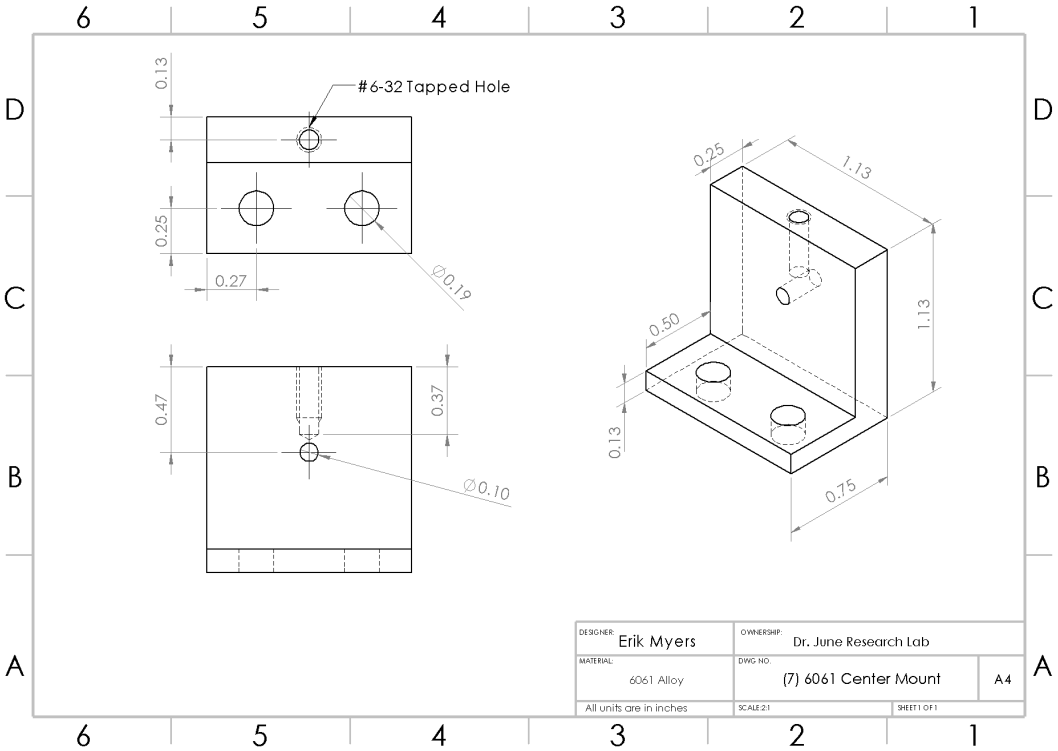
#6-32 Tapped Hole
0.13
0.25
0.27
∅0.19
0.47
0.37
∅0.10
0.25
1.13
1.13
0.50
0.13
0.75
DESIGNER: Erik Myers
OWNERSHIP: Dr. June Research Lab
MATERIAL: 6061 Alloy
DWG NO. (7) 6061 Center Mount
A4
All units are in inches
SCALE:2:1
SHEET 1 OF 1

375

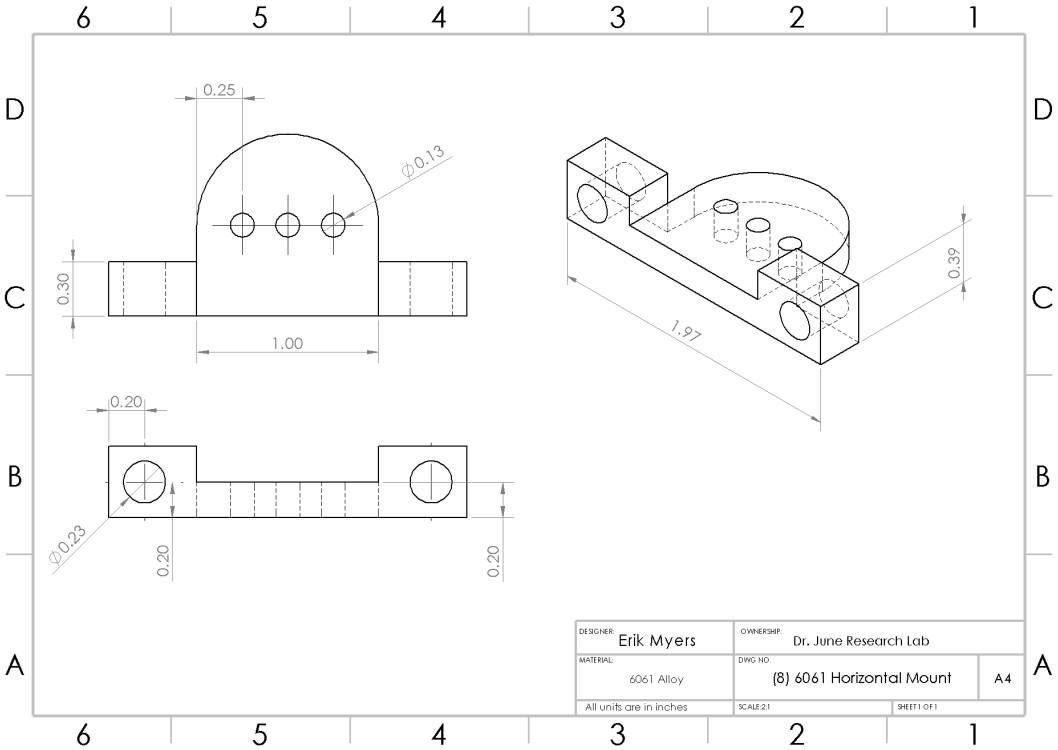
0.25
∅0.13
0.30
1.00
0.20
∅0.23
0.20
0.20
0.39
1.97
DESIGNER: Erik Myers
OWNERSHIP: Dr. June Research Lab
MATERIAL: 6061 Alloy
DWG NO. (8) 6061 Horizontal Mount
A4
All units are in inches
SCALE:2:1
SHEET 1 OF 1

376

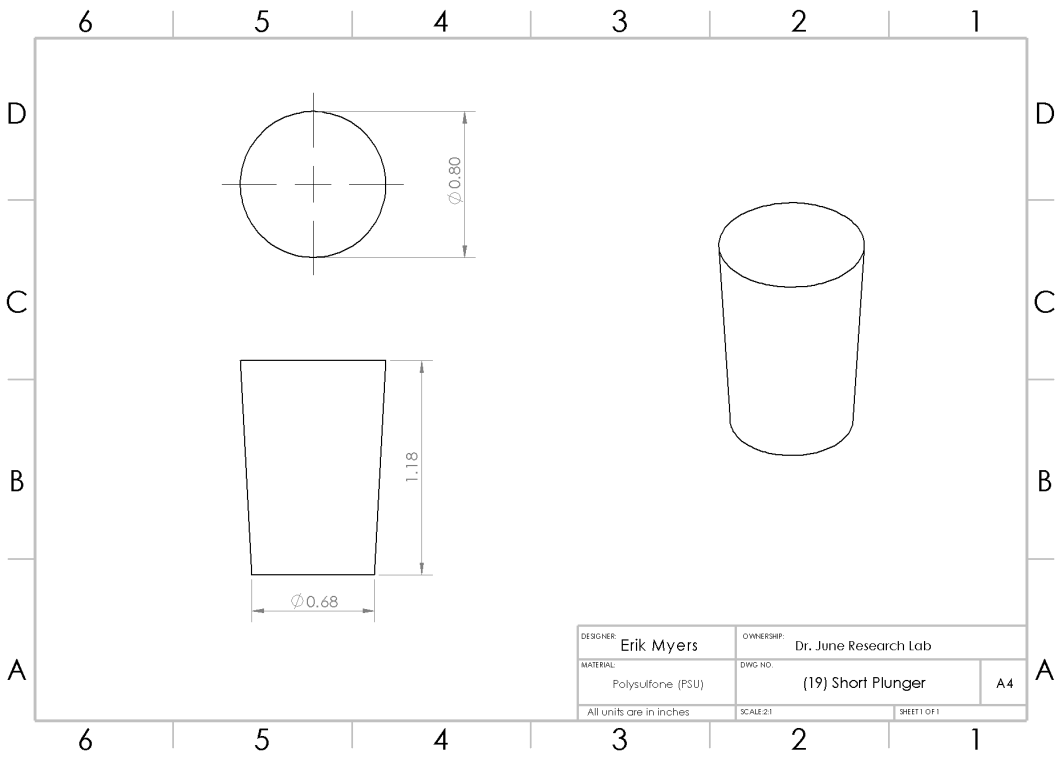

B: Metabolite Extraction and Factor Analysis

During the process of metabolite extraction, it was discovered that the previously used protocol extraction buffer (70:30:1% Methenol:Acetone:HCl) created a film in the supernatant which could clog the electro-spray ionization nozzle within the mass spectrometry machine. After the extraction of the first four donors with this method, the buffer was switched to the current buffer (70:30:1% Methanol:Acetone:Formic acid). Unfortunately, Donors #1 was unable to be cleaned substantially with the use of acetonitrile dilutions and column filtering and were subsequently removed from the data set. Donors #3 and #4 were able to be rescued using the same technique of HPLC Water:Acetonitrile dilution and column filtering with centrifugal spinning, but the results of their mass spectrometry analysis differ from the remaining 12 donors in particular metabolite concentrations.

Since three of the remaining 14 samples were extracted using a different extraction buffer (Donors 2,3, and 4), a preliminary analysis was performed using MetaboAnalyst to discover if there were concerning differences in the reported results from the mass spectrometry analysis. A Principal Component Analysis (PCA) was performed that showed immediate obvious separations between groups (Figure 3.42).

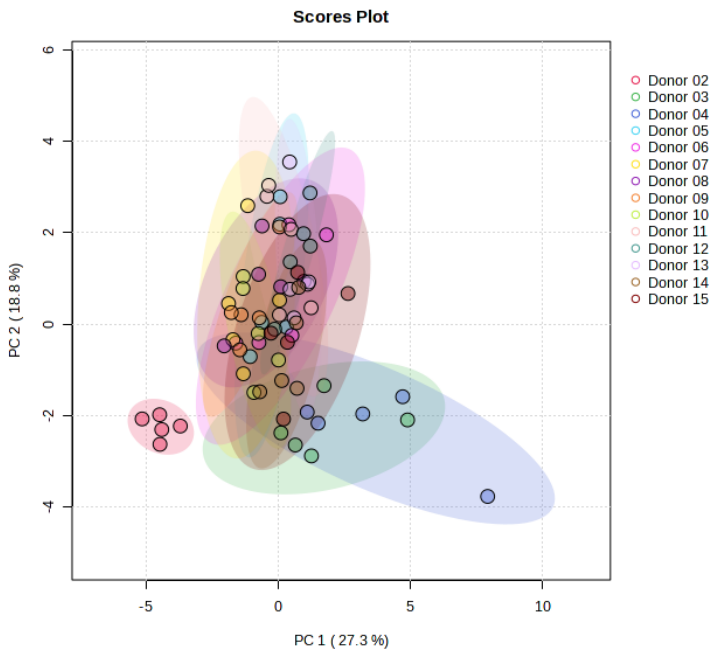

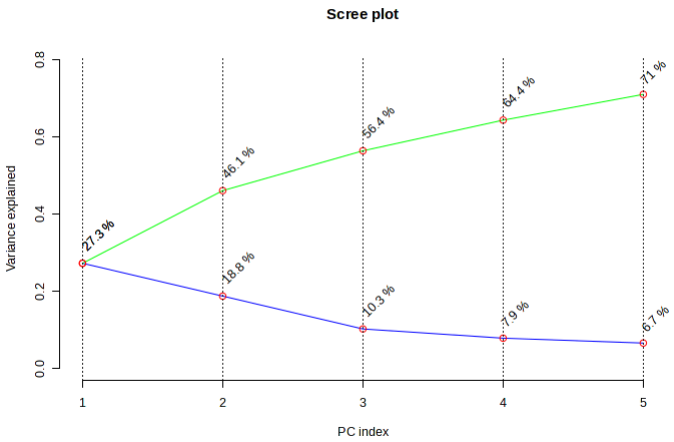

Figure 4.1: (Top) PCA analysis on a per-donor basis revealed differences between Donor 2 and the remaining donor conglomerate. Donors 3 and 4 also showed some separation but were included in the study due to significant overlap in groupings. (Bottom) Scree plot showing contribution of principal components, with 46.1% of variance being explained in the first two components.

Donor 2 showed clear differences when compared to other groups in the first two principal components, which explains 46.1% of the variance in the donor data sets. This result was concerning enough to prompt the removal of donor 2 from the dataset. Additionally, a dendrogram of the donor groupings also suggested donor 2 was clearly separated from the other donors.

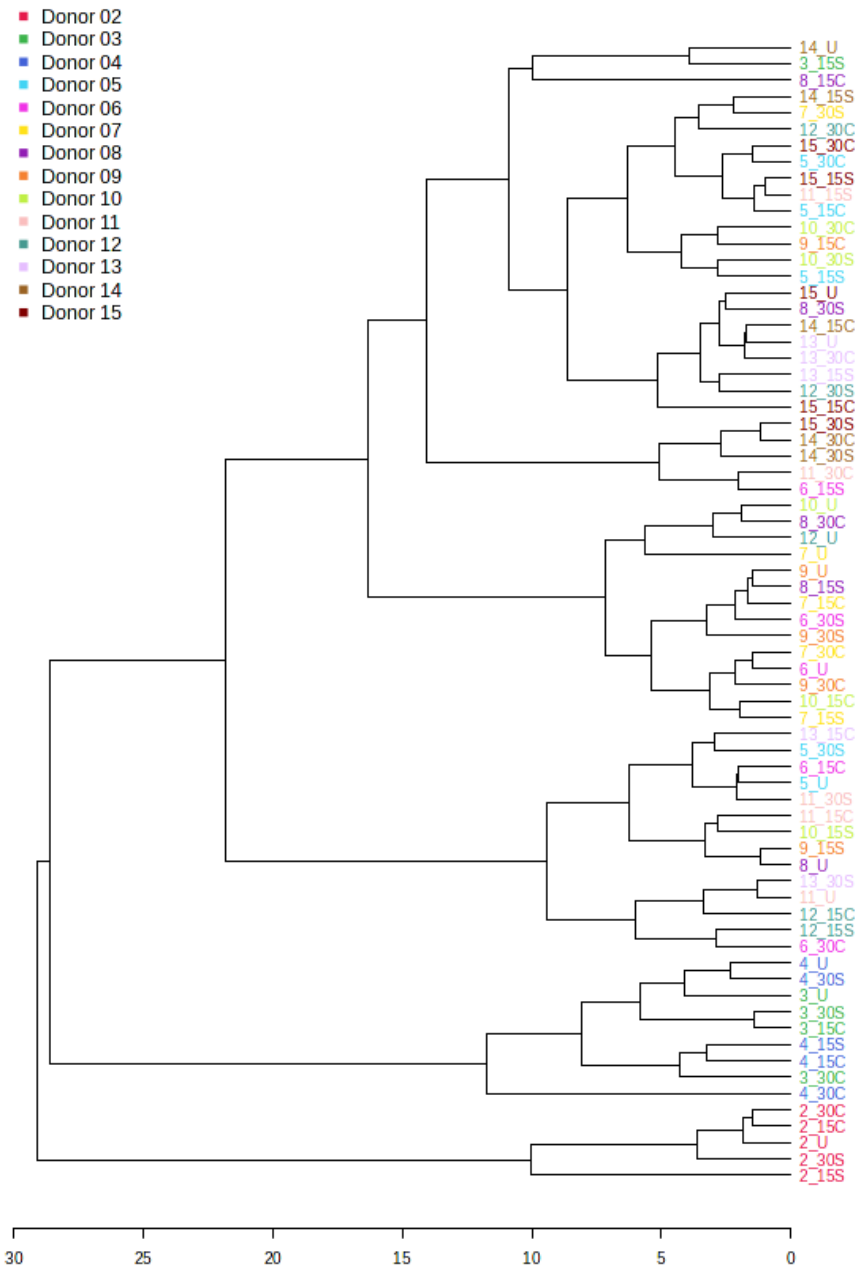

Figure 4.2: Donor 2 not only grouped exclusively with itself, but also showed greater magnitude of separation than any other grouping in the dendrogram.

Once donor #2 had been removed from the dataset, analyses were re-run to see the apparent differences in donors 2 and 3 from the remainder of the dataset (Figure 4.4).

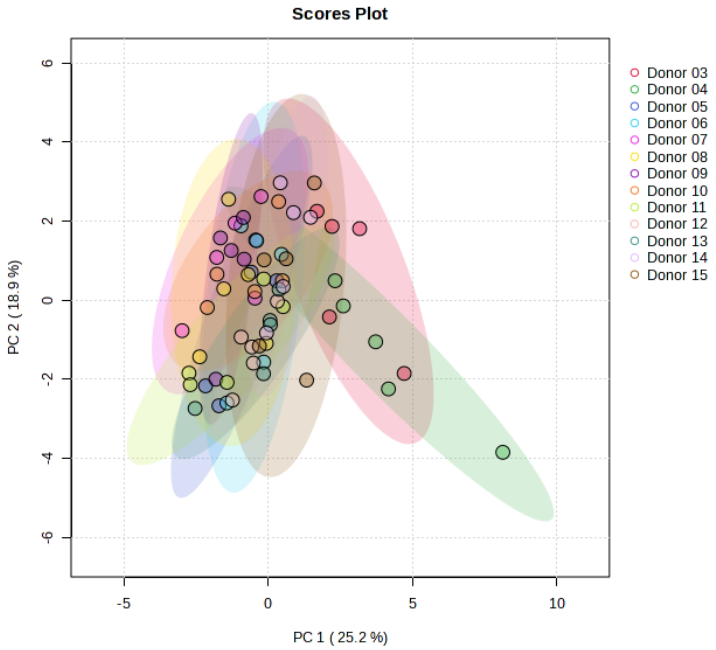

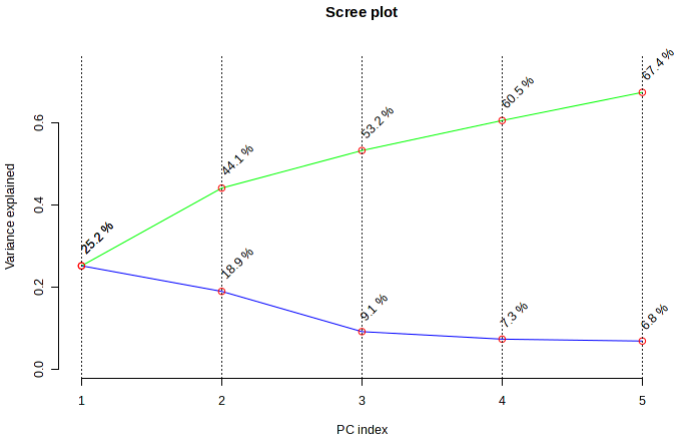

Figure 4.3: (Top) PCA of trimmed dataset shows separation of donors 3 and 4, but without a clear independent grouping to warrant removal from the dataset. (Bottom) Scree plot still shows a large contribution from the first 5 principal components, with 44.1% of the variance being explained with the first two components.

Donors 3 and 4 showed greater separation from the other responses once donor 2 was removed, but the resulting dendrogram suggested the differences were not as pronounced (Figure 3.45).

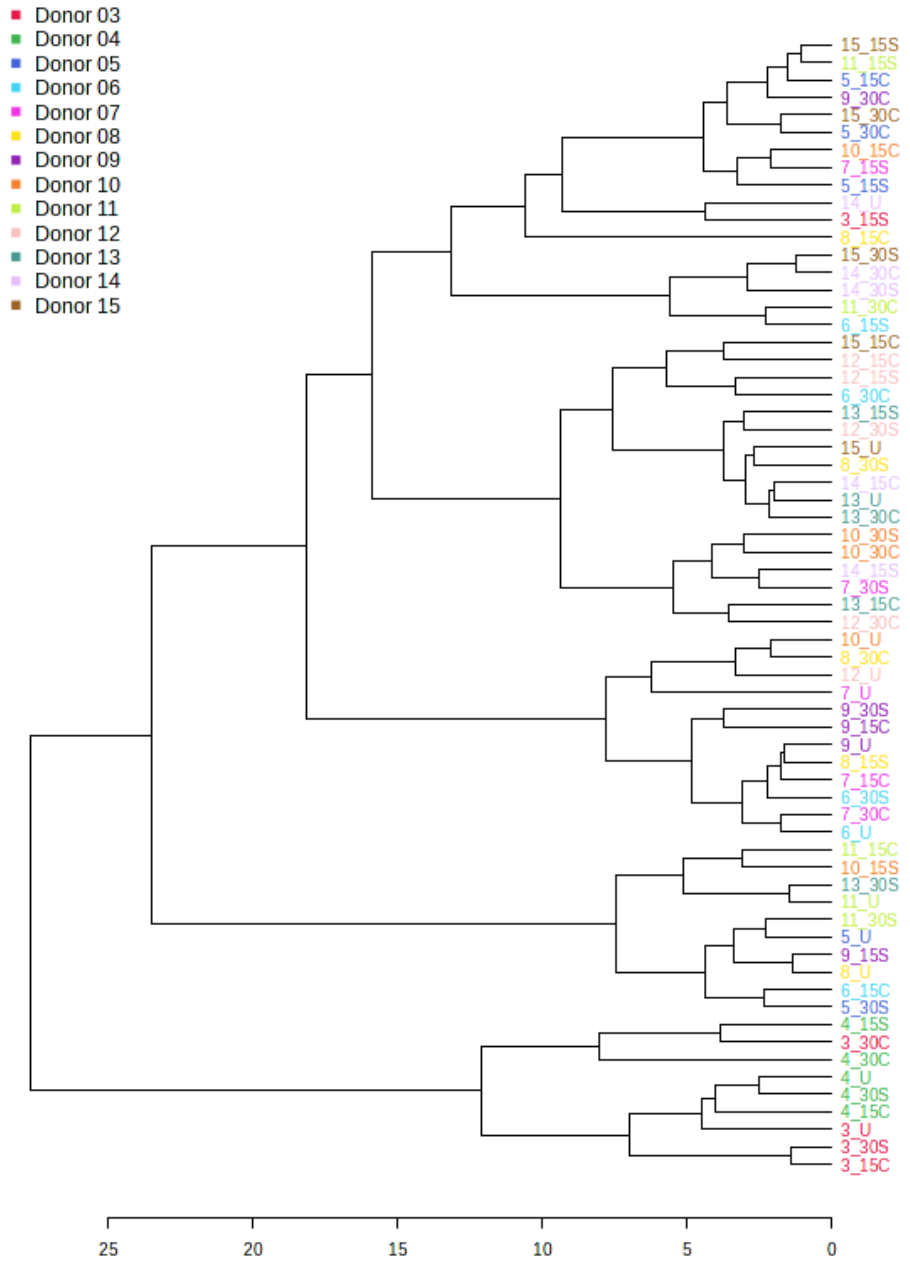

Figure 4.4: Dendrogram of the trimmed dataset shows grouping of donors 3 and 4. However, the Euclidian distance is relatively small in comparison to the separation seen by donor 2, suggesting that donors 3 and 4 may not be different enough to remove from the dataset.

Given the results of the initial donor PCA and dendrograms, the decision was made to exclude donor 2 from the dataset moving forward. This is the trimmed dataset with N=13 bovine and human donors.

Since 1/3 of the initial donor set was comprised of bovine cells (Donors 11-15), it was necessary to assess the effect of species on data grouping. If there was enough evidence to suggest that human and bovine donors reacted differently to mechanical stimulation, further statistical analyses would require species separation. Again, a PCA was performed to explore differences in metabolite profiles in a two-dimensional projection based on species (Figure 3.46).

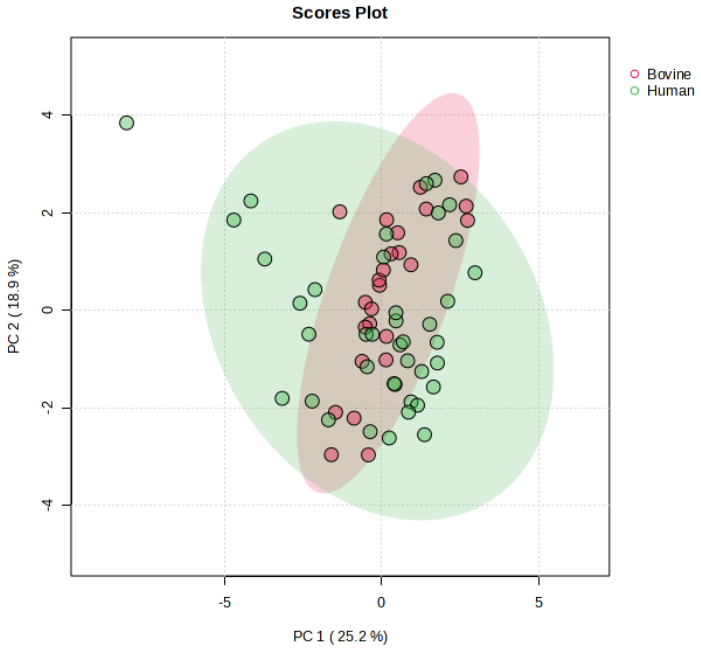

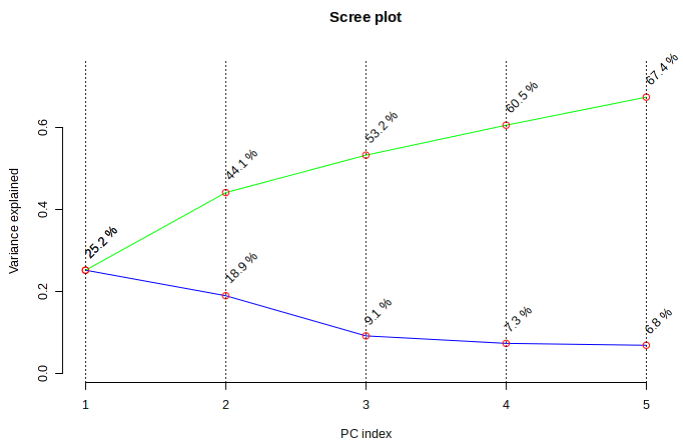

Figure 4.5: (Top) PCA analysis of species-based variation revealed considerable overlap between human and bovine donors, with 44.1% of the total variance explained in the first two components. (Bottom) Scree plot shows percentage of variation explained by five principal components.

While Figure 3.46 did demonstrate different variation in the first PC the overlap in the variance of human samples when compared to bovine donors, the overlap of groups suggests that there is not a difference between human and bovine donors. The larger variance of the human samples in the first PC is most likely because human donors are different in many aspects including age, race, sex, weight, and OA progression at the time of joint donation. Bovine donors, for the most part, are very uniform in age, sex, weight, and health at the time of donation. Regardless, the results of the PCA suggest that human and bovine donors can be treated as similar in future statistical analyses.

Before the metabolite-specific statistical analyses could be performed, final analyses were performed and differences based on the donor gender in the metabolic response profiles were explored to determine if there were effects on metabolic response based on donor gender (Figure 3.47).

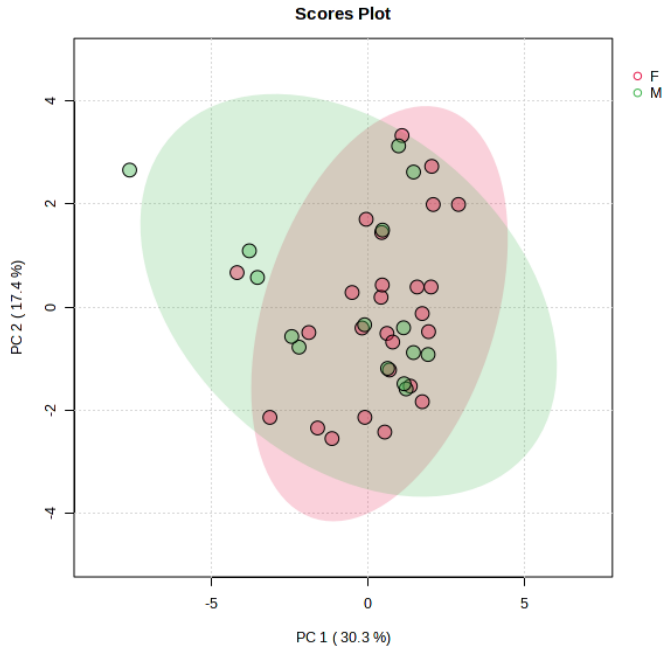

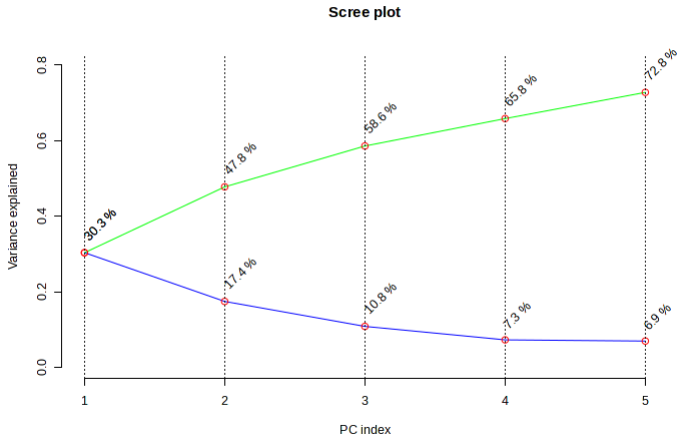

Figure 4.6: (Top) Gender-based PCA showed significant overlap and similarities in variation between male and female donors. (Bottom) Scree plot shows even greater contribution of first two principal components, explaining 47.8% of total variance.

It should be noted that the gender-based comparison was performed only with the remaining nine human donors, since the sex of bovine donors is unknown. A median

heatmap was also used to check for trends in differences between male and female donors for metabolite concentrations (Figure 4.9).

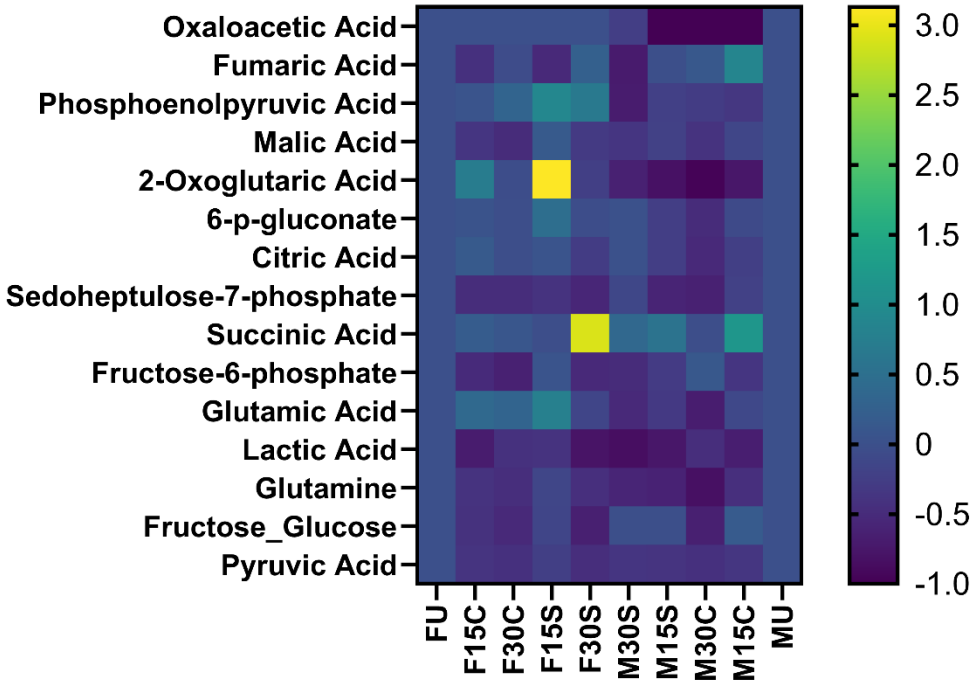

Figure 4.7: Median heatmap of group metabolite intensities separated by sex reveals no concerning differences between male and female. Group median intensities are normalized versus the unloaded control intensity. Oxaloacetate showed decreased median values for all male donors, but this trend is due to the very poor signal quality of oxaloacetate.

Based on the evidence from Figure 3.46 and Figure 3.47, it was decided to perform individual metabolite statistics with all male human, female human, and bovine samples together.

C: Mass Spectrometry Metabolite Calibration Curves

Quantitative Analysis Calibration Report

Agilent | Trusted Answers

Batch Data Path	J:\6538\shared\20241016_01_Eric_TCAcells_BEHC18-100\QuantResults\20241016_EMPB.batch.bin		
Analysis Time Stamp	10/17/2024 2:51:43 PM	**Analyst Name**	MSU\w68p731
Report Generation Time	10/17/2024 3:01:12 PM	**Reporter Name**	MSU\w68p731
Calibration Last Update	10/17/2024 2:44:43 PM	**Batch State**	Processed
Analyze Quant Version	12.0	**Report Quant Version**	12.0

Oxaloacetic acid **Relative Standard Error** 19.5

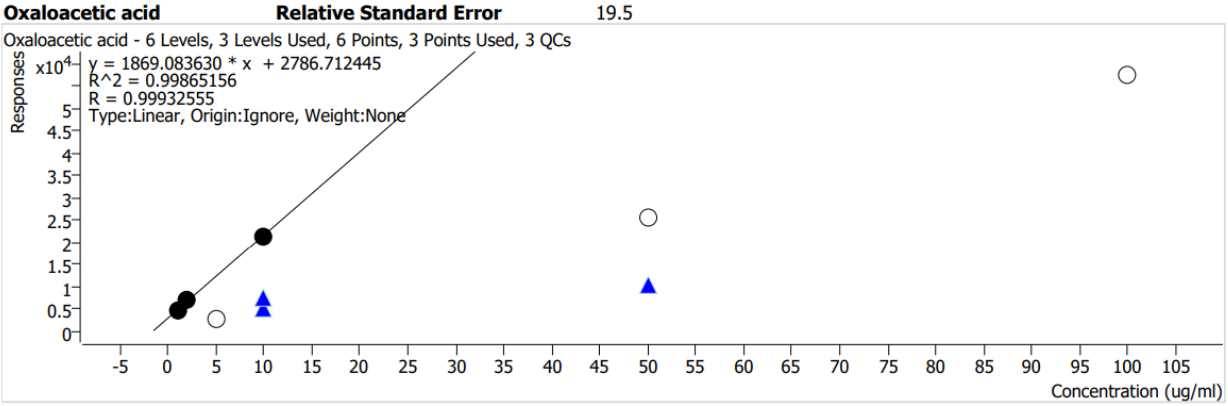

Calibration STD Path	Type	Level	Enable	Conc.	Response	RF	Level RSD
J:\6538\shared\20241016_01_Eric_TCAcells_BEHC18-100\20241016_EMPB__05_1_Std.d	Calibration	1	x	1.0000	4339	4338.5718	
J:\6538\shared\20241016_01_Eric_TCAcells_BEHC18-100\20241016_EMPB__05_2_Std.d	Calibration	2	x	2.0000	6882	3440.8785	
J:\6538\shared\20241016_01_Eric_TCAcells_BEHC18-100\20241016_EMPB__05_5_Std.d	Calibration	5		5.0000	2830	565.9365	
J:\6538\shared\20241016_01_Eric_TCAcells_BEHC18-100\20241016_EMPB__04_10_Std.d	Calibration	10	x	10.0000	21438	2143.7896	
J:\6538\shared\20241016_01_Eric_TCAcells_BEHC18-100\20241016_EMPB__88_10_Std.d	QC	10	x	10.0000	5040	503.9518	25.1
J:\6538\shared\20241016_01_Eric_TCAcells_BEHC18-100\20241017_EMPB__00_10_Std.d	QC	10	x	10.0000	7216	721.5529	25.1
J:\6538\shared\20241016_01_Eric_TCAcells_BEHC18-100\20241016_EMPB__03_50_Std.d	Calibration	50		50.0000	25400	507.9989	
J:\6538\shared\20241016_01_Eric_TCAcells_BEHC18-100\20241016_EMPB__87_50_Std.d	QC	50	x	50.0000	10401	208.0238	
J:\6538\shared\20241016_01_Eric_TCAcells_BEHC18-100\20241016_EMPB__02_100_Std.d	Calibration	100		100.0000	57204	572.0359	

Quantitative Analysis Calibration Report

Agilent | Trusted Answers

Batch Data Path	J:\6538\shared\20241016_01_Eric_TCAcells_BEHC18-100\QuantResults\20241016_EMPB.batch.bin		
Analysis Time Stamp	10/17/2024 2:51:43 PM	**Analyst Name**	MSU\w68p731
Report Generation Time	10/17/2024 3:01:12 PM	**Reporter Name**	MSU\w68p731
Calibration Last Update	10/17/2024 2:44:43 PM	**Batch State**	Processed
Analyze Quant Version	12.0	**Report Quant Version**	12.0

Fumaric acid **Relative Standard Error** 63.3

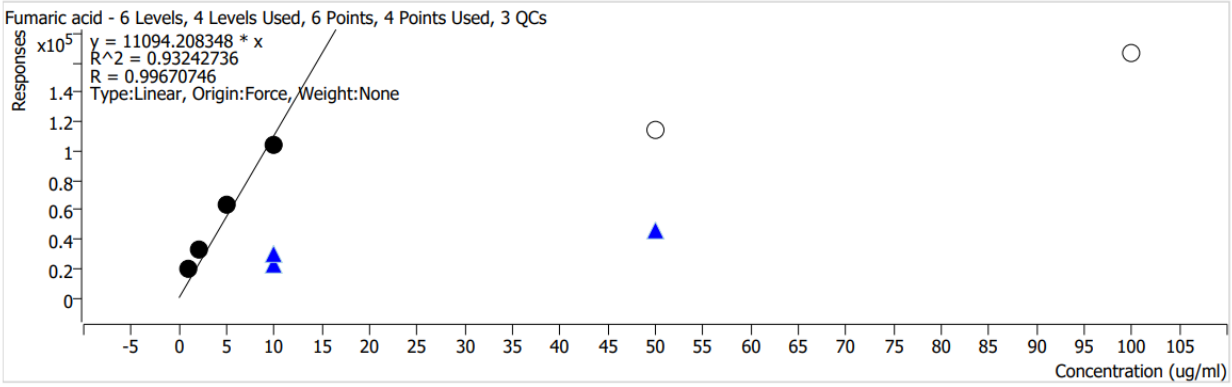

Calibration STD Path	Type	Level	Enable	Conc.	Response	RF	Level RSD
J:\6538\shared\20241016_01_Eric_TCAcells_BEHC18-100\20241016_EMPB__05_1_Std.d	Calibration	1	x	1.0000	19313	19313.2350	
J:\6538\shared\20241016_01_Eric_TCAcells_BEHC18-100\20241016_EMPB__05_2_Std.d	Calibration	2	x	2.0000	32785	16392.4565	
J:\6538\shared\20241016_01_Eric_TCAcells_BEHC18-100\20241016_EMPB__05_5_Std.d	Calibration	5	x	5.0000	63249	12649.7619	
J:\6538\shared\20241016_01_Eric_TCAcells_BEHC18-100\20241016_EMPB__04_10_Std.d	Calibration	10	x	10.0000	104112	10411.1998	
J:\6538\shared\20241016_01_Eric_TCAcells_BEHC18-100\20241016_EMPB__88_10_Std.d	QC	10	x	10.0000	22830	2283.0124	17.6
J:\6538\shared\20241016_01_Eric_TCAcells_BEHC18-100\20241017_EMPB__00_10_Std.d	QC	10	x	10.0000	29339	2933.9388	17.6
J:\6538\shared\20241016_01_Eric_TCAcells_BEHC18-100\20241016_EMPB__03_50_Std.d	Calibration	50		50.0000	114409	2288.1841	
J:\6538\shared\20241016_01_Eric_TCAcells_BEHC18-100\20241016_EMPB__87_50_Std.d	QC	50	x	50.0000	46163	923.2534	
J:\6538\shared\20241016_01_Eric_TCAcells_BEHC18-100\20241016_EMPB__02_100_Std.d	Calibration	100		100.0000	166094	1660.9379	

472

Quantitative Analysis Calibration Report

Agilent | Trusted Answers

Batch Data Path	J:\6538\shared\20241016_01_Eric_TCAcells_BEHC18-100\QuantResults\20241016_EMPB.batch.bin		
Analysis Time Stamp	10/17/2024 2:51:43 PM	**Analyst Name**	MSU\w68p731
Report Generation Time	10/17/2024 3:01:12 PM	**Reporter Name**	MSU\w68p731
Calibration Last Update	10/17/2024 2:44:43 PM	**Batch State**	Processed
Analyze Quant Version	12.0	**Report Quant Version**	12.0

Phosphoenol pyruvic acid **Relative Standard Error** 92.9

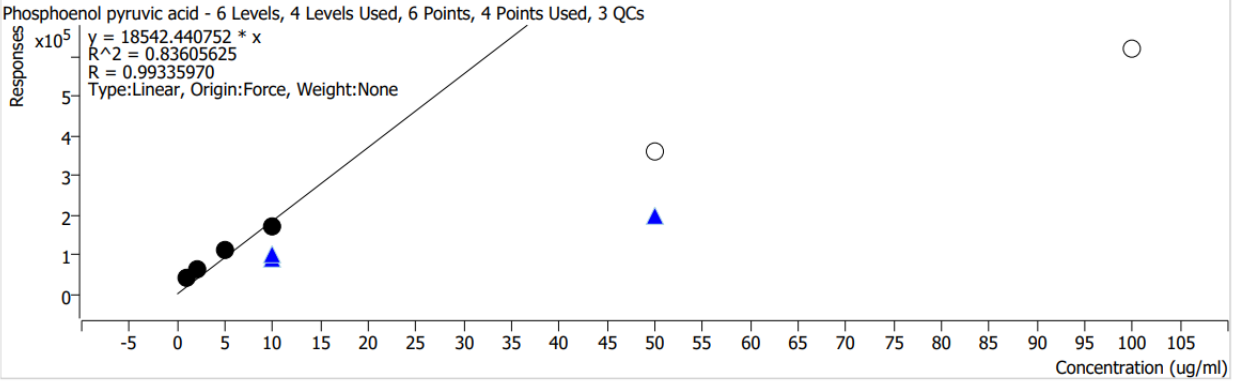

Calibration STD Path	Type	Level	Enable	Conc.	Response	RF	Level RSD
J:\6538\shared\20241016_01_Eric_TCAcells_BEHC18-100\20241016_EMPB__05_1_Std.d	Calibration	1	x	1.0000	38922	38921.6693	
J:\6538\shared\20241016_01_Eric_TCAcells_BEHC18-100\20241016_EMPB__05_2_Std.d	Calibration	2	x	2.0000	62609	31304.4547	
J:\6538\shared\20241016_01_Eric_TCAcells_BEHC18-100\20241016_EMPB__05_5_Std.d	Calibration	5	x	5.0000	110393	22078.5255	
J:\6538\shared\20241016_01_Eric_TCAcells_BEHC18-100\20241016_EMPB__04_10_Std.d	Calibration	10	x	10.0000	169441	16944.1467	
J:\6538\shared\20241016_01_Eric_TCAcells_BEHC18-100\20241016_EMPB__88_10_Std.d	QC	10	x	10.0000	91142	9114.2201	5.3
J:\6538\shared\20241016_01_Eric_TCAcells_BEHC18-100\20241017_EMPB__00_10_Std.d	QC	10	x	10.0000	98246	9824.5547	5.3
J:\6538\shared\20241016_01_Eric_TCAcells_BEHC18-100\20241016_EMPB__03_50_Std.d	Calibration	50		50.0000	358953	7179.0538	
J:\6538\shared\20241016_01_Eric_TCAcells_BEHC18-100\20241016_EMPB__87_50_Std.d	QC	50	x	50.0000	195611	3912.2131	
J:\6538\shared\20241016_01_Eric_TCAcells_BEHC18-100\20241016_EMPB__02_100_Std.d	Calibration	100		100.0000	618005	6180.0474	

473

Quantitative Analysis Calibration Report

Agilent | Trusted Answers

Batch Data Path	J:\6538\shared\20241016_01_Eric_TCAcells_BEHC18-100\QuantResults\20241016_EMPB.batch.bin		
Analysis Time Stamp	10/17/2024 2:51:43 PM	**Analyst Name**	MSU\w68p731
Report Generation Time	10/17/2024 3:01:12 PM	**Reporter Name**	MSU\w68p731
Calibration Last Update	10/17/2024 2:44:43 PM	**Batch State**	Processed
Analyze Quant Version	12.0	**Report Quant Version**	12.0

Malic acid **Relative Standard Error** 702.9

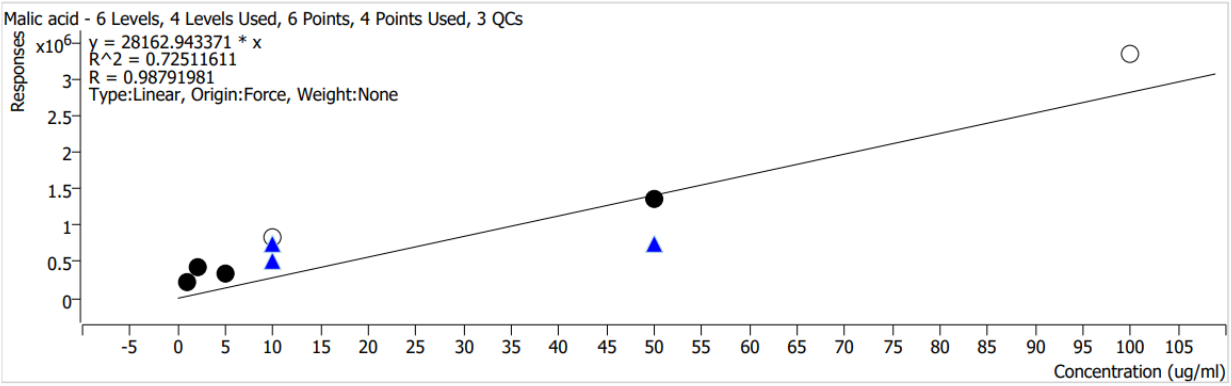

Calibration STD Path	Type	Level	Enable	Conc.	Response	RF	Level RSD
J:\6538\shared\20241016_01_Eric_TCAcells_BEHC18-100\20241016_EMPB__05_1_Std.d	Calibration	1	x	1.0000	230497	230496.8239	
J:\6538\shared\20241016_01_Eric_TCAcells_BEHC18-100\20241016_EMPB__05_2_Std.d	Calibration	2	x	2.0000	434882	217441.0116	
J:\6538\shared\20241016_01_Eric_TCAcells_BEHC18-100\20241016_EMPB__05_5_Std.d	Calibration	5	x	5.0000	341166	68233.1080	
J:\6538\shared\20241016_01_Eric_TCAcells_BEHC18-100\20241016_EMPB__04_10_Std.d	Calibration	10		10.0000	832618	83261.8434	
J:\6538\shared\20241016_01_Eric_TCAcells_BEHC18-100\20241016_EMPB__88_10_Std.d	QC	10	x	10.0000	515318	51531.7608	26.6
J:\6538\shared\20241016_01_Eric_TCAcells_BEHC18-100\20241017_EMPB__00_10_Std.d	QC	10	x	10.0000	754162	75416.1743	26.6
J:\6538\shared\20241016_01_Eric_TCAcells_BEHC18-100\20241016_EMPB__03_50_Std.d	Calibration	50	x	50.0000	1368923	27378.4633	
J:\6538\shared\20241016_01_Eric_TCAcells_BEHC18-100\20241016_EMPB__87_50_Std.d	QC	50	x	50.0000	752517	15050.3378	
J:\6538\shared\20241016_01_Eric_TCAcells_BEHC18-100\20241016_EMPB__02_100_Std.d	Calibration	100		100.0000	3328353	33283.5306	

Quantitative Analysis Calibration Report

Agilent | Trusted Answers

Batch Data Path	J:\6538\shared\20241016_01_Eric_TCAcells_BEHC18-100\QuantResults\20241016_EMPB.batch.bin		
Analysis Time Stamp	10/17/2024 2:51:43 PM	**Analyst Name**	MSU\w68p731
Report Generation Time	10/17/2024 3:01:12 PM	**Reporter Name**	MSU\w68p731
Calibration Last Update	10/17/2024 2:44:43 PM	**Batch State**	Processed
Analyze Quant Version	12.0	**Report Quant Version**	12.0

2-oxoglutaric acid **Relative Standard Error** 127.5

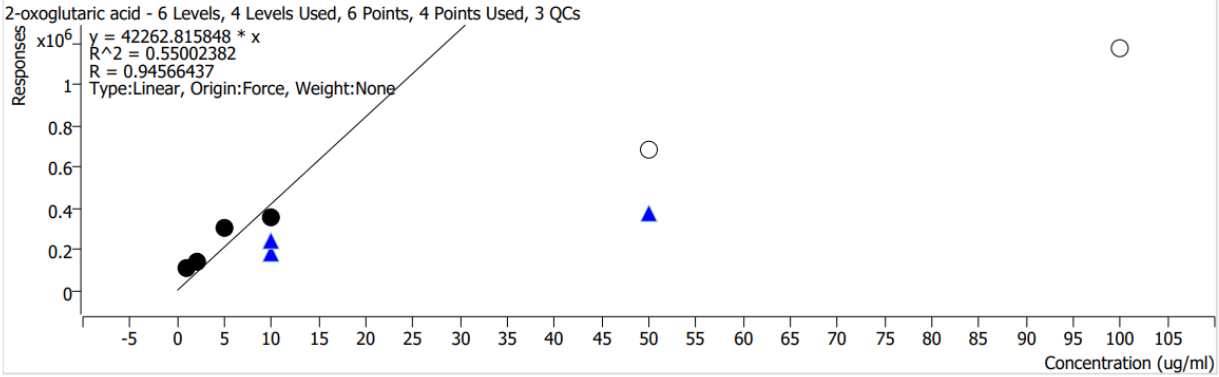

Calibration STD Path	Type	Level	Enable	Conc.	Response	RF	Level RSD
J:\6538\shared\20241016_01_Eric_TCAcells_BEHC18-100\20241016_EMPB__05_1_Std.d	Calibration	1	x	1.0000	110469	110469.4405	
J:\6538\shared\20241016_01_Eric_TCAcells_BEHC18-100\20241016_EMPB__05_2_Std.d	Calibration	2	x	2.0000	140790	70395.1849	
J:\6538\shared\20241016_01_Eric_TCAcells_BEHC18-100\20241016_EMPB__05_5_Std.d	Calibration	5	x	5.0000	301094	60218.8013	
J:\6538\shared\20241016_01_Eric_TCAcells_BEHC18-100\20241016_EMPB__04_10_Std.d	Calibration	10	x	10.0000	359665	35966.4585	
J:\6538\shared\20241016_01_Eric_TCAcells_BEHC18-100\20241016_EMPB__88_10_Std.d	QC	10	x	10.0000	177139	17713.9404	21.0
J:\6538\shared\20241016_01_Eric_TCAcells_BEHC18-100\20241017_EMPB__00_10_Std.d	QC	10	x	10.0000	238920	23892.0076	21.0
J:\6538\shared\20241016_01_Eric_TCAcells_BEHC18-100\20241016_EMPB__03_50_Std.d	Calibration	50		50.0000	689329	13786.5735	
J:\6538\shared\20241016_01_Eric_TCAcells_BEHC18-100\20241016_EMPB__87_50_Std.d	QC	50	x	50.0000	372107	7442.1371	
J:\6538\shared\20241016_01_Eric_TCAcells_BEHC18-100\20241016_EMPB__02_100_Std.d	Calibration	100		100.0000	1173641	11736.4149	

Quantitative Analysis Calibration Report

Agilent | Trusted Answers

Batch Data Path	J:\6538\shared\20241016_01_Eric_TCAcells_BEHC18-100\QuantResults\20241016_EMPB.batch.bin		
Analysis Time Stamp	10/17/2024 2:51:43 PM	**Analyst Name**	MSU\w68p731
Report Generation Time	10/17/2024 3:01:12 PM	**Reporter Name**	MSU\w68p731
Calibration Last Update	10/17/2024 2:44:43 PM	**Batch State**	Processed
Analyze Quant Version	12.0	**Report Quant Version**	12.0

6-p-gluconate **Relative Standard Error** 48.7

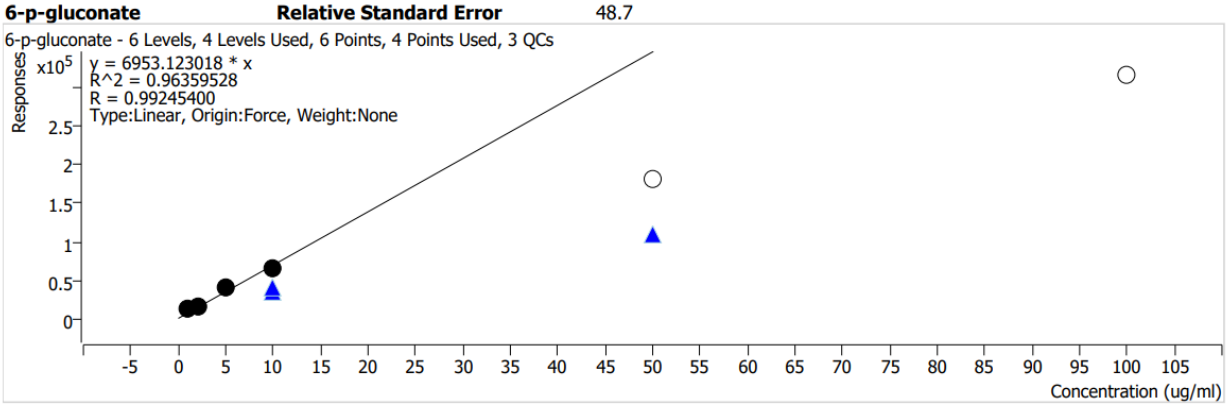

Calibration STD Path	Type	Level	Enable	Conc.	Response	RF	Level RSD
J:\6538\shared\20241016_01_Eric_TCAcells_BEHC18-100\20241016_EMPB__05_1_Std.d	Calibration	1	x	1.0000	11551	11550.6892	
J:\6538\shared\20241016_01_Eric_TCAcells_BEHC18-100\20241016_EMPB__05_2_Std.d	Calibration	2	x	2.0000	14890	7444.9646	
J:\6538\shared\20241016_01_Eric_TCAcells_BEHC18-100\20241016_EMPB__05_5_Std.d	Calibration	5	x	5.0000	40688	8137.6027	
J:\6538\shared\20241016_01_Eric_TCAcells_BEHC18-100\20241016_EMPB__04_10_Std.d	Calibration	10	x	10.0000	65914	6591.3538	
J:\6538\shared\20241016_01_Eric_TCAcells_BEHC18-100\20241016_EMPB__88_10_Std.d	QC	10	x	10.0000	34092	3409.1531	13.4
J:\6538\shared\20241016_01_Eric_TCAcells_BEHC18-100\20241017_EMPB__00_10_Std.d	QC	10	x	10.0000	41224	4122.4235	13.4
J:\6538\shared\20241016_01_Eric_TCAcells_BEHC18-100\20241016_EMPB__03_50_Std.d	Calibration	50		50.0000	180628	3612.5537	
J:\6538\shared\20241016_01_Eric_TCAcells_BEHC18-100\20241016_EMPB__87_50_Std.d	QC	50	x	50.0000	109010	2180.1951	
J:\6538\shared\20241016_01_Eric_TCAcells_BEHC18-100\20241016_EMPB__02_100_Std.d	Calibration	100		100.0000	316522	3165.2152	

Quantitative Analysis Calibration Report

Agilent | Trusted Answers

Batch Data Path	J:\6538\shared\20241016_01_Eric_TCAcells_BEHC18-100\QuantResults\20241016_EMPB.batch.bin		
Analysis Time Stamp	10/17/2024 2:51:43 PM	**Analyst Name**	MSU\w68p731
Report Generation Time	10/17/2024 3:01:12 PM	**Reporter Name**	MSU\w68p731
Calibration Last Update	10/17/2024 2:44:43 PM	**Batch State**	Processed
Analyze Quant Version	12.0	**Report Quant Version**	12.0

Citric acid **Relative Standard Error** 141.8

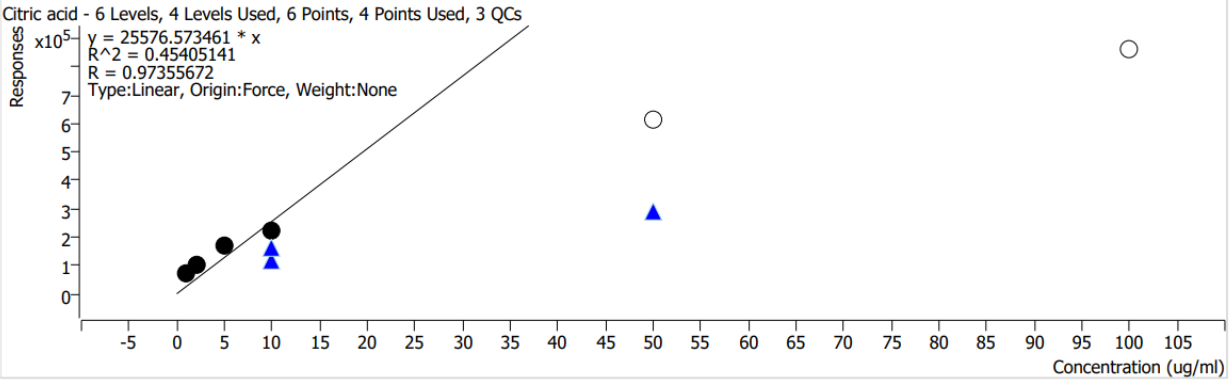

Calibration STD Path	Type	Level	Enable	Conc.	Response	RF	Level RSD
J:\6538\shared\20241016_01_Eric_TCAcells_BEHC18-100\20241016_EMPB__05_1_Std.d	Calibration	1	x	1.0000	68773	68773.0530	
J:\6538\shared\20241016_01_Eric_TCAcells_BEHC18-100\20241016_EMPB__05_2_Std.d	Calibration	2	x	2.0000	103483	51741.4495	
J:\6538\shared\20241016_01_Eric_TCAcells_BEHC18-100\20241016_EMPB__05_5_Std.d	Calibration	5	x	5.0000	168564	33712.7097	
J:\6538\shared\20241016_01_Eric_TCAcells_BEHC18-100\20241016_EMPB__04_10_Std.d	Calibration	10	x	10.0000	220640	22063.9796	
J:\6538\shared\20241016_01_Eric_TCAcells_BEHC18-100\20241016_EMPB__88_10_Std.d	QC	10	x	10.0000	120100	12009.9917	22.2
J:\6538\shared\20241016_01_Eric_TCAcells_BEHC18-100\20241017_EMPB__00_10_Std.d	QC	10	x	10.0000	164786	16478.6083	22.2
J:\6538\shared\20241016_01_Eric_TCAcells_BEHC18-100\20241016_EMPB__03_50_Std.d	Calibration	50		50.0000	616142	12322.8408	
J:\6538\shared\20241016_01_Eric_TCAcells_BEHC18-100\20241016_EMPB__87_50_Std.d	QC	50	x	50.0000	287487	5749.7379	
J:\6538\shared\20241016_01_Eric_TCAcells_BEHC18-100\20241016_EMPB__02_100_Std.d	Calibration	100		100.0000	858937	8589.3657	

477

Quantitative Analysis Calibration Report

Agilent | Trusted Answers

Batch Data Path	J:\6538\shared\20241016_01_Eric_TCAcells_BEHC18-100\QuantResults\20241016_EMPB.batch.bin		
Analysis Time Stamp	10/17/2024 2:51:43 PM	**Analyst Name**	MSU\w68p731
Report Generation Time	10/17/2024 3:01:12 PM	**Reporter Name**	MSU\w68p731
Calibration Last Update	10/17/2024 2:44:43 PM	**Batch State**	Processed
Analyze Quant Version	12.0	**Report Quant Version**	12.0

sedoheptulose-7-phosphate **Relative Standard Error** 131.6

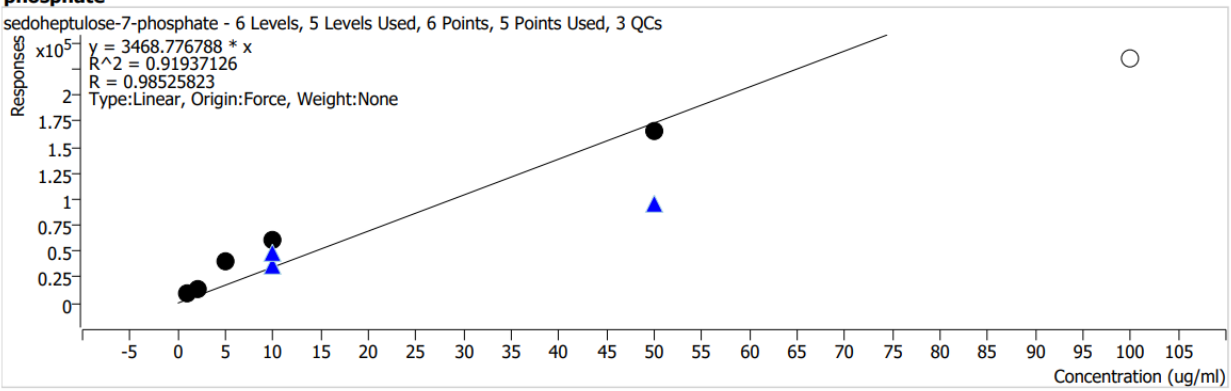

Calibration STD Path	Type	Level	Enable	Conc.	Response	RF	Level RSD
J:\6538\shared\20241016_01_Eric_TCAcells_BEHC18-100\20241016_EMPB__05_1_Std.d	Calibration	1	x	1.0000	8513	8512.8089	
J:\6538\shared\20241016_01_Eric_TCAcells_BEHC18-100\20241016_EMPB__05_2_Std.d	Calibration	2	x	2.0000	13249	6624.4038	
J:\6538\shared\20241016_01_Eric_TCAcells_BEHC18-100\20241016_EMPB__05_5_Std.d	Calibration	5	x	5.0000	39798	7959.5605	
J:\6538\shared\20241016_01_Eric_TCAcells_BEHC18-100\20241016_EMPB__04_10_Std.d	Calibration	10	x	10.0000	60929	6092.9112	
J:\6538\shared\20241016_01_Eric_TCAcells_BEHC18-100\20241016_EMPB__88_10_Std.d	QC	10	x	10.0000	36018	3601.8028	20.5
J:\6538\shared\20241016_01_Eric_TCAcells_BEHC18-100\20241017_EMPB__00_10_Std.d	QC	10	x	10.0000	48245	4824.4706	20.5
J:\6538\shared\20241016_01_Eric_TCAcells_BEHC18-100\20241016_EMPB__03_50_Std.d	Calibration	50	x	50.0000	165592	3311.8370	
J:\6538\shared\20241016_01_Eric_TCAcells_BEHC18-100\20241016_EMPB__87_50_Std.d	QC	50	x	50.0000	94825	1896.4907	
J:\6538\shared\20241016_01_Eric_TCAcells_BEHC18-100\20241016_EMPB__02_100_Std.d	Calibration	100		100.0000	234760	2347.6043	

478

Quantitative Analysis Calibration Report

Agilent | Trusted Answers

Batch Data Path	J:\6538\shared\20241016_01_Eric_TCAcells_BEHC18-100\QuantResults\20241016_EMPB.batch.bin		
Analysis Time Stamp	10/17/2024 2:51:43 PM	**Analyst Name**	MSU\w68p731
Report Generation Time	10/17/2024 3:01:12 PM	**Reporter Name**	MSU\w68p731
Calibration Last Update	10/17/2024 2:44:43 PM	**Batch State**	Processed
Analyze Quant Version	12.0	**Report Quant Version**	12.0

Succinic acid **Relative Standard Error** 28.5

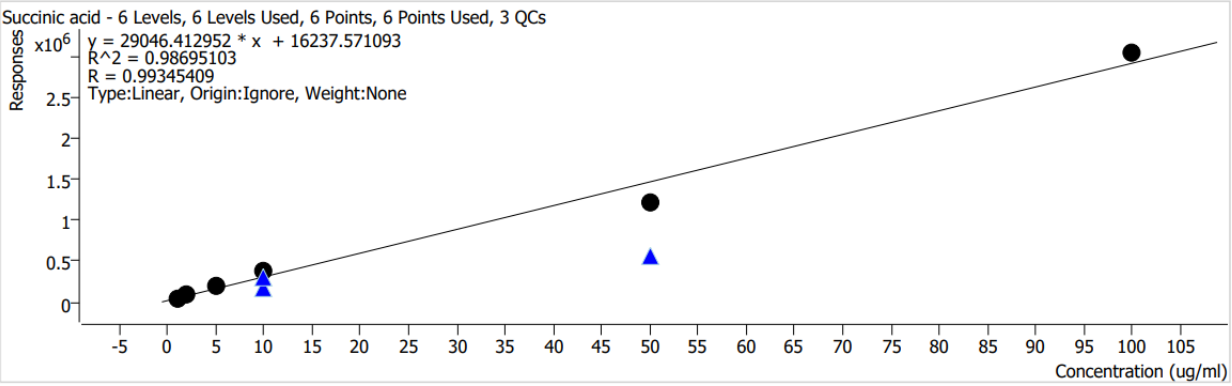

Calibration STD Path	Type	Level	Enable	Conc.	Response	RF	Level RSD
J:\6538\shared\20241016_01_Eric_TCAcells_BEHC18-100\20241016_EMPB__05_1_Std.d	Calibration	1	x	1.0000	50746	50746.0617	
J:\6538\shared\20241016_01_Eric_TCAcells_BEHC18-100\20241016_EMPB__05_2_Std.d	Calibration	2	x	2.0000	95487	47743.3427	
J:\6538\shared\20241016_01_Eric_TCAcells_BEHC18-100\20241016_EMPB__05_5_Std.d	Calibration	5	x	5.0000	193268	38653.6478	
J:\6538\shared\20241016_01_Eric_TCAcells_BEHC18-100\20241016_EMPB__04_10_Std.d	Calibration	10	x	10.0000	387204	38720.3677	
J:\6538\shared\20241016_01_Eric_TCAcells_BEHC18-100\20241016_EMPB__88_10_Std.d	QC	10	x	10.0000	167171	16717.1130	42.1
J:\6538\shared\20241016_01_Eric_TCAcells_BEHC18-100\20241017_EMPB__00_10_Std.d	QC	10	x	10.0000	309095	30909.5335	42.1
J:\6538\shared\20241016_01_Eric_TCAcells_BEHC18-100\20241016_EMPB__03_50_Std.d	Calibration	50	x	50.0000	1210956	24219.1215	
J:\6538\shared\20241016_01_Eric_TCAcells_BEHC18-100\20241016_EMPB__87_50_Std.d	QC	50	x	50.0000	571050	11420.9950	
J:\6538\shared\20241016_01_Eric_TCAcells_BEHC18-100\20241016_EMPB__02_100_Std.d	Calibration	100	x	100.0000	3039562	30395.6206	

Quantitative Analysis Calibration Report

Agilent | Trusted Answers

Batch Data Path	J:\6538\shared\20241016_01_Eric_TCAcells_BEHC18-100\QuantResults\20241016_EMPB.batch.bin		
Analysis Time Stamp	10/17/2024 2:51:43 PM	**Analyst Name**	MSU\w68p731
Report Generation Time	10/17/2024 3:01:12 PM	**Reporter Name**	MSU\w68p731
Calibration Last Update	10/17/2024 2:44:43 PM	**Batch State**	Processed
Analyze Quant Version	12.0	**Report Quant Version**	12.0

Fructose-6-phosphate **Relative Standard Error** 138.0

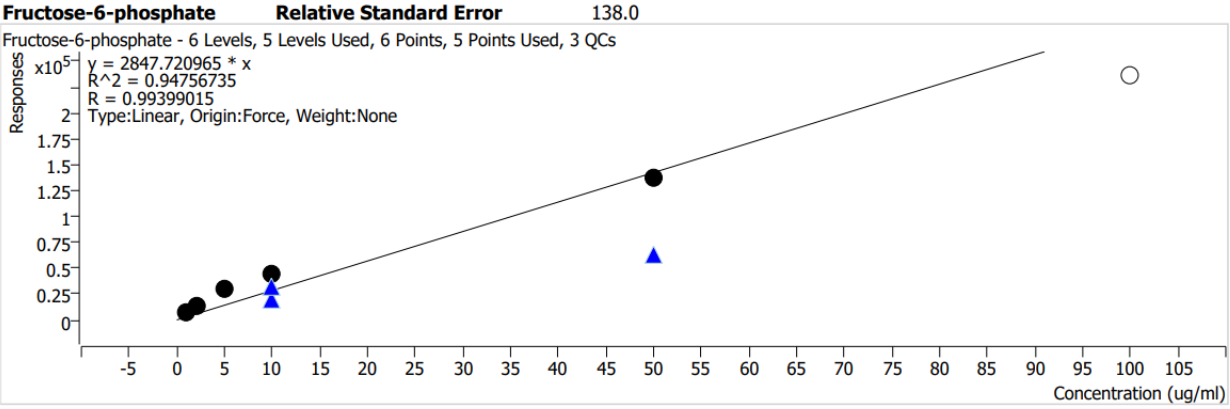

Calibration STD Path	Type	Level	Enable	Conc.	Response	RF	Level RSD
J:\6538\shared\20241016_01_Eric_TCAcells_BEHC18-100\20241016_EMPB__05_1_Std.d	Calibration	1	x	1.0000	6752	6751.6727	
J:\6538\shared\20241016_01_Eric_TCAcells_BEHC18-100\20241016_EMPB__05_2_Std.d	Calibration	2	x	2.0000	14596	7298.1885	
J:\6538\shared\20241016_01_Eric_TCAcells_BEHC18-100\20241016_EMPB__05_5_Std.d	Calibration	5	x	5.0000	29113	5822.5066	
J:\6538\shared\20241016_01_Eric_TCAcells_BEHC18-100\20241016_EMPB__04_10_Std.d	Calibration	10	x	10.0000	44094	4409.4108	
J:\6538\shared\20241016_01_Eric_TCAcells_BEHC18-100\20241016_EMPB__88_10_Std.d	QC	10	x	10.0000	19865	1986.5162	34.9
J:\6538\shared\20241016_01_Eric_TCAcells_BEHC18-100\20241017_EMPB__00_10_Std.d	QC	10	x	10.0000	32874	3287.3763	34.9
J:\6538\shared\20241016_01_Eric_TCAcells_BEHC18-100\20241016_EMPB__03_50_Std.d	Calibration	50	x	50.0000	137341	2746.8232	
J:\6538\shared\20241016_01_Eric_TCAcells_BEHC18-100\20241016_EMPB__87_50_Std.d	QC	50	x	50.0000	63368	1267.3590	
J:\6538\shared\20241016_01_Eric_TCAcells_BEHC18-100\20241016_EMPB__02_100_Std.d	Calibration	100		100.0000	235551	2355.5105	

480

Quantitative Analysis Calibration Report

Agilent | Trusted Answers

Batch Data Path	J:\6538\shared\20241016_01_Eric_TCAcells_BEHC18-100\QuantResults\20241016_EMPB.batch.bin		
Analysis Time Stamp	10/17/2024 2:51:43 PM	**Analyst Name**	MSU\w68p731
Report Generation Time	10/17/2024 3:01:12 PM	**Reporter Name**	MSU\w68p731
Calibration Last Update	10/17/2024 2:44:43 PM	**Batch State**	Processed
Analyze Quant Version	12.0	**Report Quant Version**	12.0

Glutamic Acid **Relative Standard Error** 291.6

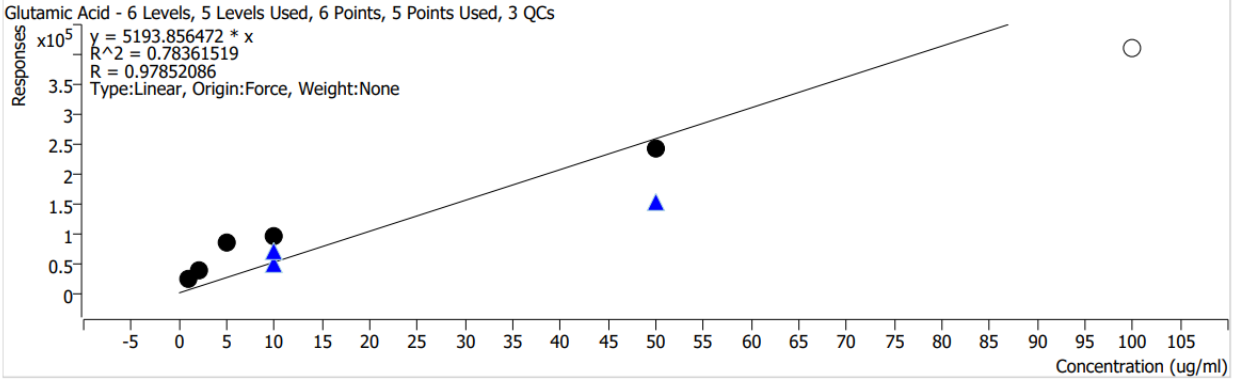

Calibration STD Path	Type	Level	Enable	Conc.	Response	RF	Level RSD
J:\6538\shared\20241016_01_Eric_TCAcells_BEHC18-100\20241016_EMPB__05_1_Std.d	Calibration	1	x	1.0000	24178	24177.5898	
J:\6538\shared\20241016_01_Eric_TCAcells_BEHC18-100\20241016_EMPB__05_2_Std.d	Calibration	2	x	2.0000	36698	18349.1413	
J:\6538\shared\20241016_01_Eric_TCAcells_BEHC18-100\20241016_EMPB__05_5_Std.d	Calibration	5	x	5.0000	84141	16828.2844	
J:\6538\shared\20241016_01_Eric_TCAcells_BEHC18-100\20241016_EMPB__04_10_Std.d	Calibration	10	x	10.0000	95877	9587.6854	
J:\6538\shared\20241016_01_Eric_TCAcells_BEHC18-100\20241016_EMPB__88_10_Std.d	QC	10	x	10.0000	50514	5051.4224	22.1
J:\6538\shared\20241016_01_Eric_TCAcells_BEHC18-100\20241017_EMPB__00_10_Std.d	QC	10	x	10.0000	69193	6919.3410	22.1
J:\6538\shared\20241016_01_Eric_TCAcells_BEHC18-100\20241016_EMPB__03_50_Std.d	Calibration	50	x	50.0000	243656	4873.1171	
J:\6538\shared\20241016_01_Eric_TCAcells_BEHC18-100\20241016_EMPB__87_50_Std.d	QC	50	x	50.0000	154818	3096.3668	
J:\6538\shared\20241016_01_Eric_TCAcells_BEHC18-100\20241016_EMPB__02_100_Std.d	Calibration	100		100.0000	410601	4106.0123	

Quantitative Analysis Calibration Report

Agilent | Trusted Answers

Batch Data Path	J:\6538\shared\20241016_01_Eric_TCAcells_BEHC18-100\QuantResults\20241016_EMPB.batch.bin		
Analysis Time Stamp	10/17/2024 2:51:43 PM	**Analyst Name**	MSU\w68p731
Report Generation Time	10/17/2024 3:01:12 PM	**Reporter Name**	MSU\w68p731
Calibration Last Update	10/17/2024 2:44:43 PM	**Batch State**	Processed
Analyze Quant Version	12.0	**Report Quant Version**	12.0

Lactic acid **Relative Standard Error** 26.8

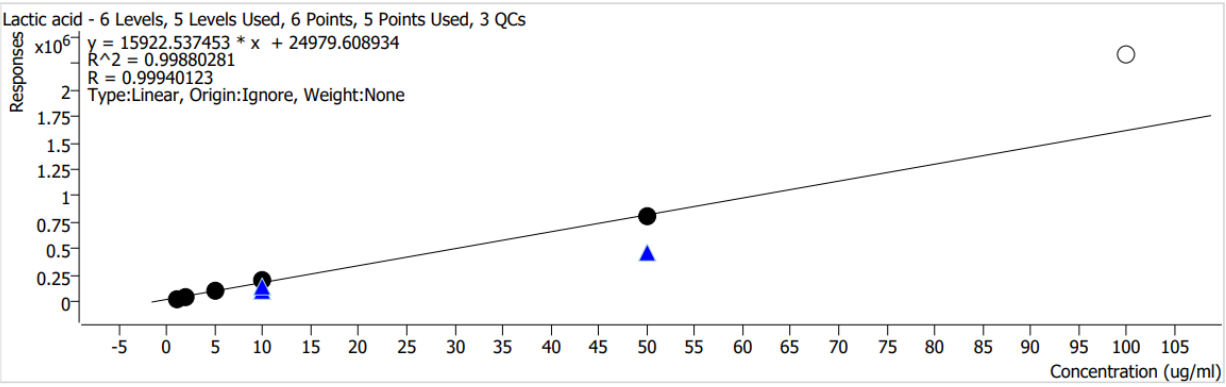

Calibration STD Path	Type	Level	Enable	Conc.	Response	RF	Level RSD
J:\6538\shared\20241016_01_Eric_TCAcells_BEHC18-100\20241016_EMPB__05_1_Std.d	Calibration	1	x	1.0000	35047	35046.5926	
J:\6538\shared\20241016_01_Eric_TCAcells_BEHC18-100\20241016_EMPB__05_2_Std.d	Calibration	2	x	2.0000	48820	24410.0634	
J:\6538\shared\20241016_01_Eric_TCAcells_BEHC18-100\20241016_EMPB__05_5_Std.d	Calibration	5	x	5.0000	101712	20342.3121	
J:\6538\shared\20241016_01_Eric_TCAcells_BEHC18-100\20241016_EMPB__04_10_Std.d	Calibration	10	x	10.0000	204224	20422.4333	
J:\6538\shared\20241016_01_Eric_TCAcells_BEHC18-100\20241016_EMPB__88_10_Std.d	QC	10	x	10.0000	111794	11179.4303	18.2
J:\6538\shared\20241016_01_Eric_TCAcells_BEHC18-100\20241017_EMPB__00_10_Std.d	QC	10	x	10.0000	144844	14484.4067	18.2
J:\6538\shared\20241016_01_Eric_TCAcells_BEHC18-100\20241016_EMPB__03_50_Std.d	Calibration	50	x	50.0000	817828	16356.5596	
J:\6538\shared\20241016_01_Eric_TCAcells_BEHC18-100\20241016_EMPB__87_50_Std.d	QC	50	x	50.0000	463901	9278.0201	
J:\6538\shared\20241016_01_Eric_TCAcells_BEHC18-100\20241016_EMPB__02_100_Std.d	Calibration	100		100.0000	2324781	23247.8112	

482

Quantitative Analysis Calibration Report

Agilent | Trusted Answers

Batch Data Path	J:\6538\shared\20241016_01_Eric_TCAcells_BEHC18-100\QuantResults\20241016_EMPB.batch.bin		
Analysis Time Stamp	10/17/2024 2:51:43 PM	**Analyst Name**	MSU\w68p731
Report Generation Time	10/17/2024 3:01:12 PM	**Reporter Name**	MSU\w68p731
Calibration Last Update	10/17/2024 2:44:43 PM	**Batch State**	Processed
Analyze Quant Version	12.0	**Report Quant Version**	12.0

Glutamine **Relative Standard Error** 99.0

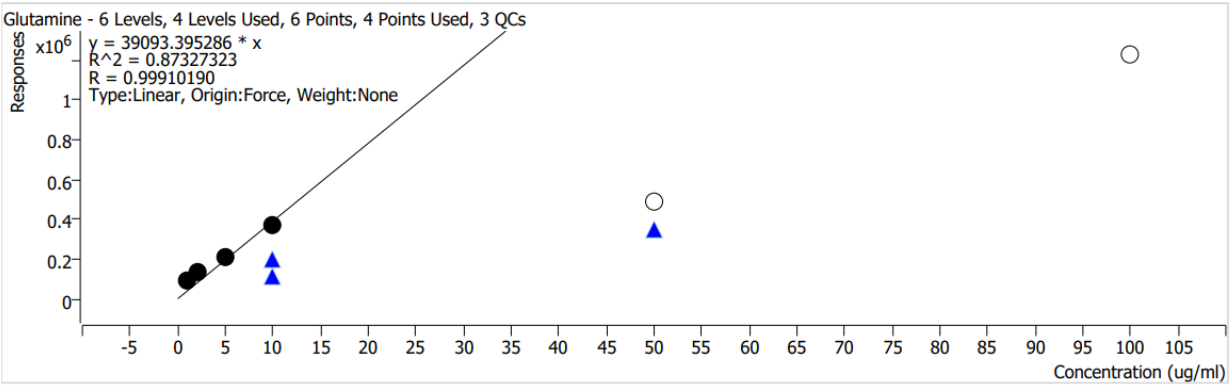

Calibration STD Path	Type	Level	Enable	Conc.	Response	RF	Level RSD
J:\6538\shared\20241016_01_Eric_TCAcells_BEHC18-100\20241016_EMPB__05_1_Std.d	Calibration	1	x	1.0000	87134	87133.7552	
J:\6538\shared\20241016_01_Eric_TCAcells_BEHC18-100\20241016_EMPB__05_2_Std.d	Calibration	2	x	2.0000	129906	64953.0716	
J:\6538\shared\20241016_01_Eric_TCAcells_BEHC18-100\20241016_EMPB__05_5_Std.d	Calibration	5	x	5.0000	212091	42418.2437	
J:\6538\shared\20241016_01_Eric_TCAcells_BEHC18-100\20241016_EMPB__04_10_Std.d	Calibration	10	x	10.0000	367474	36747.3925	
J:\6538\shared\20241016_01_Eric_TCAcells_BEHC18-100\20241016_EMPB__88_10_Std.d	QC	10	x	10.0000	111961	11196.0949	41.1
J:\6538\shared\20241016_01_Eric_TCAcells_BEHC18-100\20241017_EMPB__00_10_Std.d	QC	10	x	10.0000	203651	20365.0738	41.1
J:\6538\shared\20241016_01_Eric_TCAcells_BEHC18-100\20241016_EMPB__03_50_Std.d	Calibration	50		50.0000	488020	9760.4033	
J:\6538\shared\20241016_01_Eric_TCAcells_BEHC18-100\20241016_EMPB__87_50_Std.d	QC	50	x	50.0000	350973	7019.4623	
J:\6538\shared\20241016_01_Eric_TCAcells_BEHC18-100\20241016_EMPB__02_100_Std.d	Calibration	100		100.0000	1223898	12238.9806	

483

Quantitative Analysis Calibration Report

Agilent | Trusted Answers

Batch Data Path	J:\6538\shared\20241016_01_Eric_TCAcells_BEHC18-100\QuantResults\20241016_EMPB.batch.bin		
Analysis Time Stamp	10/17/2024 2:51:43 PM	**Analyst Name**	MSU\w68p731
Report Generation Time	10/17/2024 3:01:12 PM	**Reporter Name**	MSU\w68p731
Calibration Last Update	10/17/2024 2:44:43 PM	**Batch State**	Processed
Analyze Quant Version	12.0	**Report Quant Version**	12.0

Fructose/Glucose **Relative Standard Error** 55.4

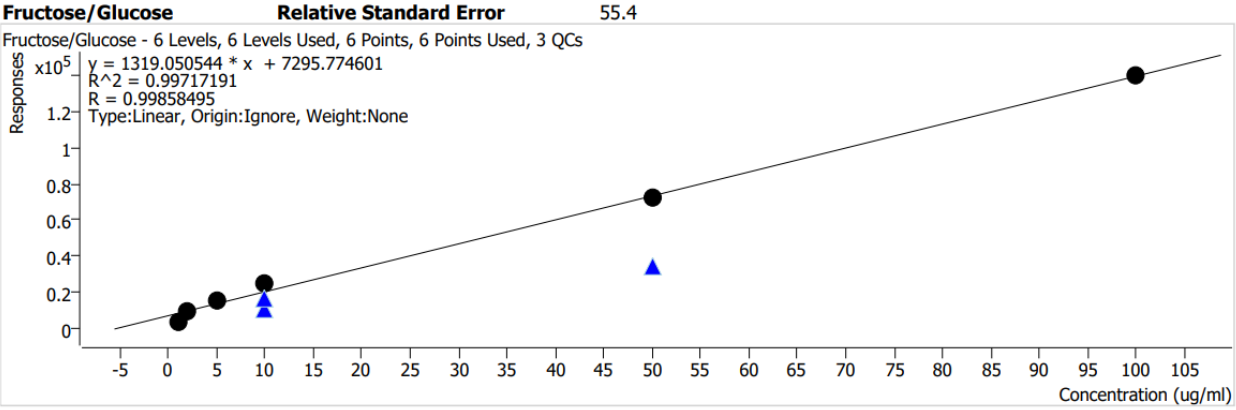

Calibration STD Path	Type	Level	Enable	Conc.	Response	RF	Level RSD
J:\6538\shared\20241016_01_Eric_TCAcells_BEHC18-100\20241016_EMPB__05_1_Std.d	Calibration	1	x	1.0000	4373	4372.7731	
J:\6538\shared\20241016_01_Eric_TCAcells_BEHC18-100\20241016_EMPB__05_2_Std.d	Calibration	2	x	2.0000	9243	4621.5065	
J:\6538\shared\20241016_01_Eric_TCAcells_BEHC18-100\20241016_EMPB__05_5_Std.d	Calibration	5	x	5.0000	15497	3099.4421	
J:\6538\shared\20241016_01_Eric_TCAcells_BEHC18-100\20241016_EMPB__04_10_Std.d	Calibration	10	x	10.0000	24658	2465.8207	
J:\6538\shared\20241016_01_Eric_TCAcells_BEHC18-100\20241016_EMPB__88_10_Std.d	QC	10	x	10.0000	10603	1060.2812	33.2
J:\6538\shared\20241016_01_Eric_TCAcells_BEHC18-100\20241017_EMPB__00_10_Std.d	QC	10	x	10.0000	17117	1711.6984	33.2
J:\6538\shared\20241016_01_Eric_TCAcells_BEHC18-100\20241016_EMPB__03_50_Std.d	Calibration	50	x	50.0000	72440	1448.8088	
J:\6538\shared\20241016_01_Eric_TCAcells_BEHC18-100\20241016_EMPB__87_50_Std.d	QC	50	x	50.0000	34731	694.6155	
J:\6538\shared\20241016_01_Eric_TCAcells_BEHC18-100\20241016_EMPB__02_100_Std.d	Calibration	100	x	100.0000	139163	1391.6350	

484

Quantitative Analysis Calibration Report

Agilent | Trusted Answers

Batch Data Path	J:\6538\shared\20241016_01_Eric_TCAcells_BEHC18-100\QuantResults\20241016_EMPB.batch.bin		
Analysis Time Stamp	10/17/2024 2:51:43 PM	**Analyst Name**	MSU\w68p731
Report Generation Time	10/17/2024 3:01:12 PM	**Reporter Name**	MSU\w68p731
Calibration Last Update	10/17/2024 2:44:43 PM	**Batch State**	Processed
Analyze Quant Version	12.0	**Report Quant Version**	12.0

Pyruvic acid **Relative Standard Error** 259.0

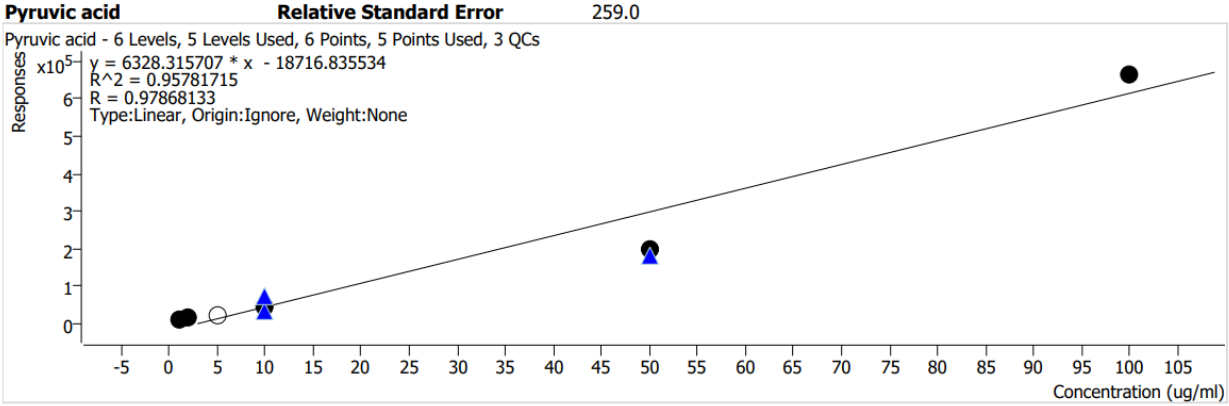

Calibration STD Path	Type	Level	Enable	Conc.	Response	RF	Level RSD
J:\6538\shared\20241016_01_Eric_TCAcells_BEHC18-100\20241016_EMPB__05_1_Std.d	Calibration	1	x	1.0000	13440	13439.7243	
J:\6538\shared\20241016_01_Eric_TCAcells_BEHC18-100\20241016_EMPB__05_2_Std.d	Calibration	2	x	2.0000	17168	8583.8982	
J:\6538\shared\20241016_01_Eric_TCAcells_BEHC18-100\20241016_EMPB__05_5_Std.d	Calibration	5		5.0000	20871	4174.1839	
J:\6538\shared\20241016_01_Eric_TCAcells_BEHC18-100\20241016_EMPB__04_10_Std.d	Calibration	10	x	10.0000	44665	4466.4658	
J:\6538\shared\20241016_01_Eric_TCAcells_BEHC18-100\20241016_EMPB__88_10_Std.d	QC	10	x	10.0000	36087	3608.6610	49.5
J:\6538\shared\20241016_01_Eric_TCAcells_BEHC18-100\20241017_EMPB__00_10_Std.d	QC	10	x	10.0000	74910	7491.0283	49.5
J:\6538\shared\20241016_01_Eric_TCAcells_BEHC18-100\20241016_EMPB__03_50_Std.d	Calibration	50	x	50.0000	200855	4017.1028	
J:\6538\shared\20241016_01_Eric_TCAcells_BEHC18-100\20241016_EMPB__87_50_Std.d	QC	50	x	50.0000	182157	3643.1356	
J:\6538\shared\20241016_01_Eric_TCAcells_BEHC18-100\20241016_EMPB__02_100_Std.d	Calibration	100	x	100.0000	661804	6618.0396	

485

Quantitative Analysis Calibration Report

Agilent | Trusted Answers

Batch Data Path	J:\6538\shared\20241016_01_Eric_TCAcells_BEHC18-100\QuantResults\20241016_EMPB.batch.bin		
Analysis Time Stamp	10/17/2024 2:51:43 PM	**Analyst Name**	MSU\w68p731
Report Generation Time	10/17/2024 3:01:12 PM	**Reporter Name**	MSU\w68p731
Calibration Last Update	10/17/2024 2:44:43 PM	**Batch State**	Processed
Analyze Quant Version	12.0	**Report Quant Version**	12.0

NADH-1 **Relative Standard Error** 547.3

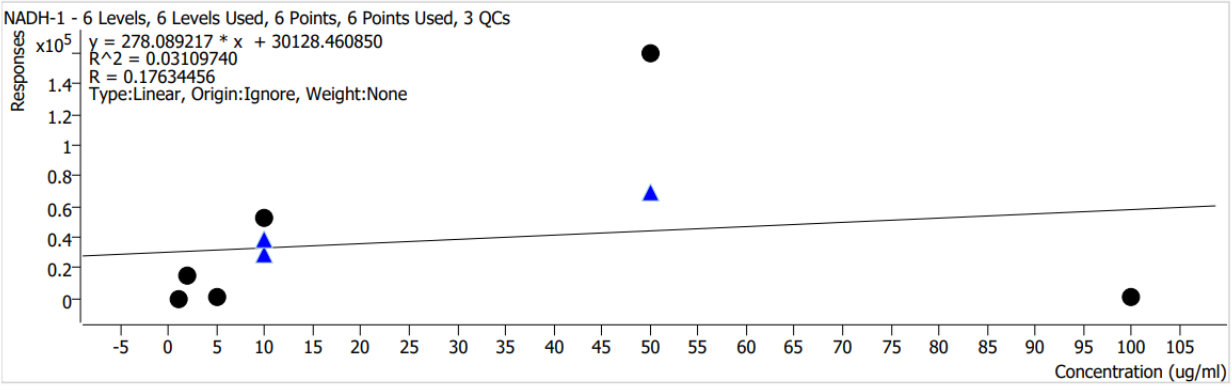

Calibration STD Path	Type	Level	Enable	Conc.	Response	RF	Level RSD
J:\6538\shared\20241016_01_Eric_TCAcells_BEHC18-100\20241016_EMPB__05_1_Std.d	Calibration	1	x	1.0000	50	50.2955	
J:\6538\shared\20241016_01_Eric_TCAcells_BEHC18-100\20241016_EMPB__05_2_Std.d	Calibration	2	x	2.0000	15096	7547.9082	
J:\6538\shared\20241016_01_Eric_TCAcells_BEHC18-100\20241016_EMPB__05_5_Std.d	Calibration	5	x	5.0000	463	92.6655	
J:\6538\shared\20241016_01_Eric_TCAcells_BEHC18-100\20241016_EMPB__04_10_Std.d	Calibration	10	x	10.0000	51966	5196.6295	
J:\6538\shared\20241016_01_Eric_TCAcells_BEHC18-100\20241016_EMPB__88_10_Std.d	QC	10	x	10.0000	29113	2911.3293	18.8
J:\6538\shared\20241016_01_Eric_TCAcells_BEHC18-100\20241017_EMPB__00_10_Std.d	QC	10	x	10.0000	38029	3802.9004	18.8
J:\6538\shared\20241016_01_Eric_TCAcells_BEHC18-100\20241016_EMPB__03_50_Std.d	Calibration	50	x	50.0000	159396	3187.9101	
J:\6538\shared\20241016_01_Eric_TCAcells_BEHC18-100\20241016_EMPB__87_50_Std.d	QC	50	x	50.0000	69470	1389.3914	
J:\6538\shared\20241016_01_Eric_TCAcells_BEHC18-100\20241016_EMPB__02_100_Std.d	Calibration	100	x	100.0000	519	5.1852	

Quantitative Analysis Calibration Report

Agilent | Trusted Answers

Batch Data Path	J:\6538\shared\20241016_01_Eric_TCAcells_BEHC18-100\QuantResults\20241016_EMPB.batch.bin		
Analysis Time Stamp	10/17/2024 2:51:43 PM	**Analyst Name**	MSU\w68p731
Report Generation Time	10/17/2024 3:01:12 PM	**Reporter Name**	MSU\w68p731
Calibration Last Update	10/17/2024 2:44:43 PM	**Batch State**	Processed
Analyze Quant Version	12.0	**Report Quant Version**	12.0

HS-CoA **Relative Standard Error** 89.3

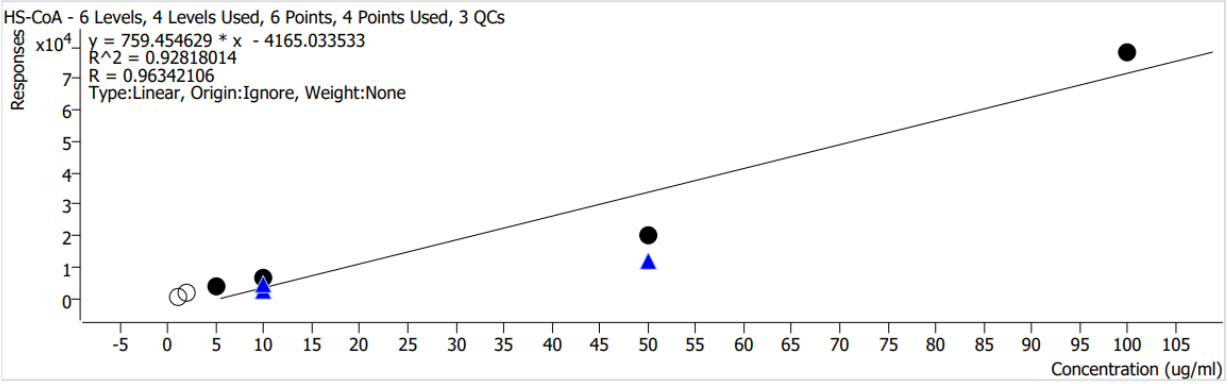

Calibration STD Path	Type	Level	Enable	Conc.	Response	RF	Level RSD
J:\6538\shared\20241016_01_Eric_TCAcells_BEHC18-100\20241016_EMPB__05_1_Std.d	Calibration	1		1.0000	765	764.6817	
J:\6538\shared\20241016_01_Eric_TCAcells_BEHC18-100\20241016_EMPB__05_2_Std.d	Calibration	2		2.0000	1921	960.6338	
J:\6538\shared\20241016_01_Eric_TCAcells_BEHC18-100\20241016_EMPB__05_5_Std.d	Calibration	5	x	5.0000	3937	787.4508	
J:\6538\shared\20241016_01_Eric_TCAcells_BEHC18-100\20241016_EMPB__04_10_Std.d	Calibration	10	x	10.0000	6557	655.7325	
J:\6538\shared\20241016_01_Eric_TCAcells_BEHC18-100\20241016_EMPB__88_10_Std.d	QC	10	x	10.0000	2797	279.7010	29.0
J:\6538\shared\20241016_01_Eric_TCAcells_BEHC18-100\20241017_EMPB__00_10_Std.d	QC	10	x	10.0000	4241	424.0736	29.0
J:\6538\shared\20241016_01_Eric_TCAcells_BEHC18-100\20241016_EMPB__03_50_Std.d	Calibration	50	x	50.0000	19998	399.9621	
J:\6538\shared\20241016_01_Eric_TCAcells_BEHC18-100\20241016_EMPB__87_50_Std.d	QC	50	x	50.0000	12275	245.5024	
J:\6538\shared\20241016_01_Eric_TCAcells_BEHC18-100\20241016_EMPB__02_100_Std.d	Calibration	100	x	100.0000	78157	781.5719	

487

Quantitative Analysis Calibration Report

Agilent | Trusted Answers

Batch Data Path	J:\6538\shared\20241016_01_Eric_TCAcells_BEHC18-100\QuantResults\20241016_EMPB.batch.bin		
Analysis Time Stamp	10/17/2024 2:51:43 PM	**Analyst Name**	MSU\w68p731
Report Generation Time	10/17/2024 3:01:12 PM	**Reporter Name**	MSU\w68p731
Calibration Last Update	10/17/2024 2:44:43 PM	**Batch State**	Processed
Analyze Quant Version	12.0	**Report Quant Version**	12.0

NADH-2 **Relative Standard Error** 206.9

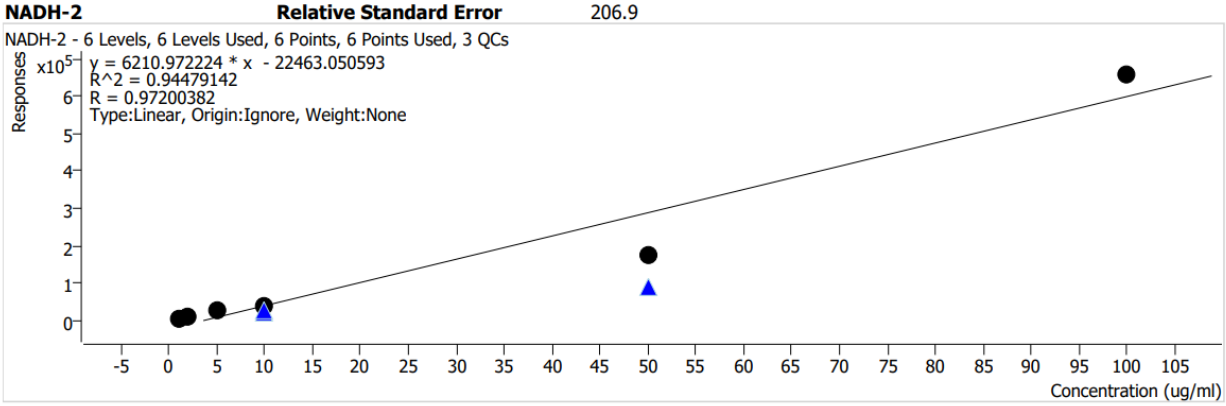

Calibration STD Path	Type	Level	Enable	Conc.	Response	RF	Level RSD
J:\6538\shared\20241016_01_Eric_TCAcells_BEHC18-100\20241016_EMPB__05_1_Std.d	Calibration	1	x	1.0000	7219	7219.3765	
J:\6538\shared\20241016_01_Eric_TCAcells_BEHC18-100\20241016_EMPB__05_2_Std.d	Calibration	2	x	2.0000	8880	4440.0325	
J:\6538\shared\20241016_01_Eric_TCAcells_BEHC18-100\20241016_EMPB__05_5_Std.d	Calibration	5	x	5.0000	27597	5519.4442	
J:\6538\shared\20241016_01_Eric_TCAcells_BEHC18-100\20241016_EMPB__04_10_Std.d	Calibration	10	x	10.0000	37466	3746.5698	
J:\6538\shared\20241016_01_Eric_TCAcells_BEHC18-100\20241016_EMPB__88_10_Std.d	QC	10	x	10.0000	22386	2238.6353	7.1
J:\6538\shared\20241016_01_Eric_TCAcells_BEHC18-100\20241017_EMPB__00_10_Std.d	QC	10	x	10.0000	24742	2474.2453	7.1
J:\6538\shared\20241016_01_Eric_TCAcells_BEHC18-100\20241016_EMPB__03_50_Std.d	Calibration	50	x	50.0000	172342	3446.8412	
J:\6538\shared\20241016_01_Eric_TCAcells_BEHC18-100\20241016_EMPB__87_50_Std.d	QC	50	x	50.0000	87213	1744.2529	
J:\6538\shared\20241016_01_Eric_TCAcells_BEHC18-100\20241016_EMPB__02_100_Std.d	Calibration	100	x	100.0000	655161	6551.6061	

488

D: Metabolite Plots where no differences were detected in initial F-test

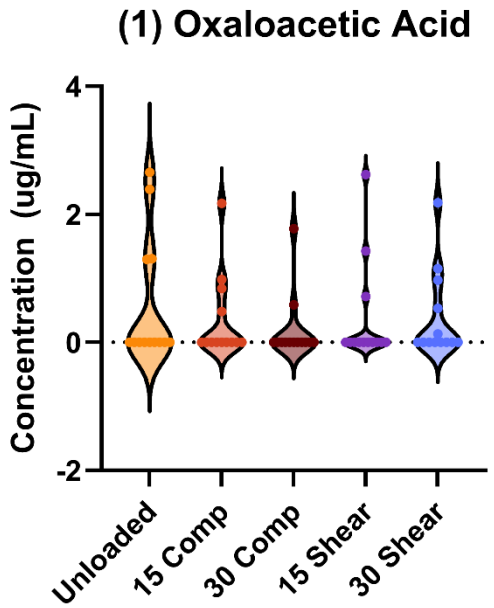

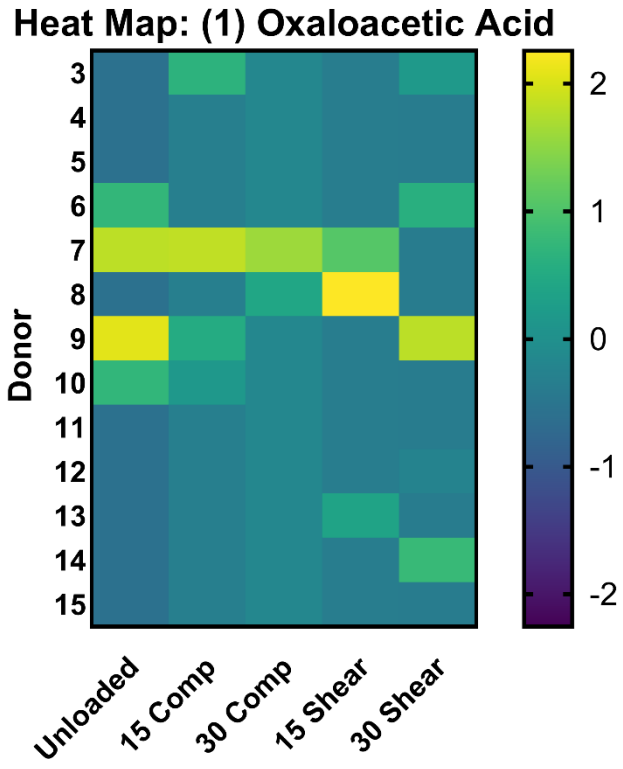

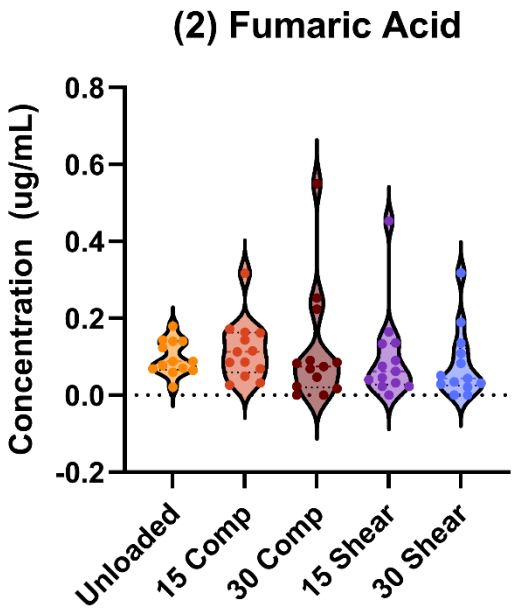
(2) Fumaric Acid
Concentration (ug/mL)
0.8
0.6
0.4
0.2
0.0
-0.2
Unloaded
15 Comp
30 Comp
15 Shear
30 Shear

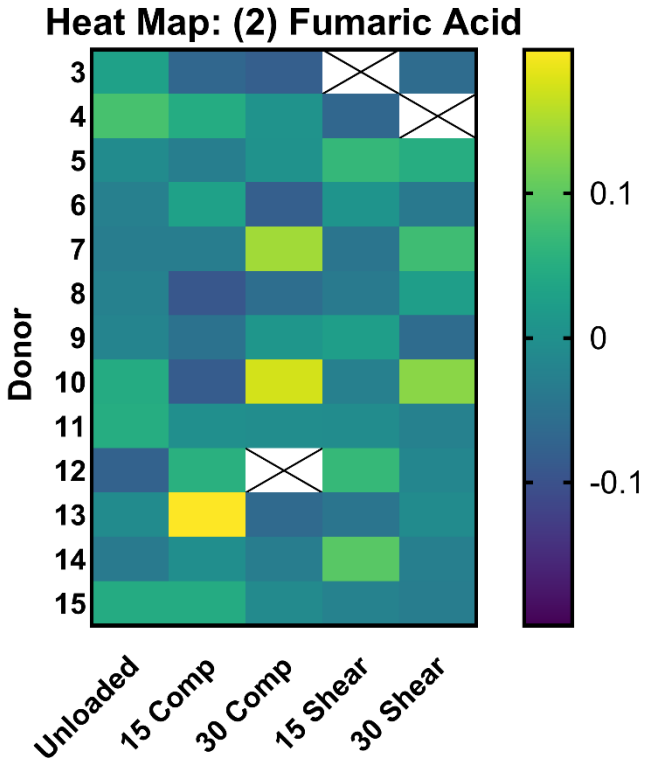
Heat Map: (2) Fumaric Acid
Donor
3
4
5
6
7
8
9
10
11
12
13
14
15
Unloaded
15 Comp
30 Comp
15 Shear
30 Shear
0.1
0
-0.1

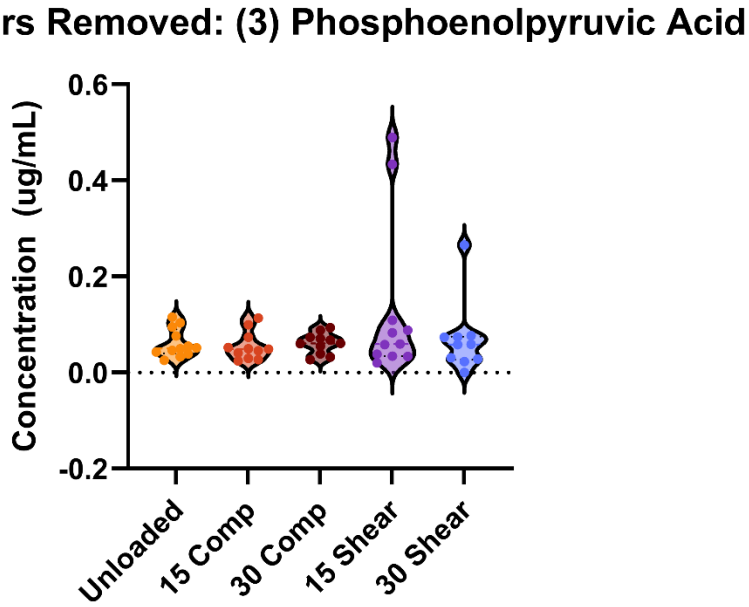
Outliers Removed: (3) Phosphoenolpyruvic Acid
Concentration (ug/mL)
0.6
0.4
0.2
0.0
-0.2
Unloaded
15 Comp
30 Comp
15 Shear
30 Shear

494

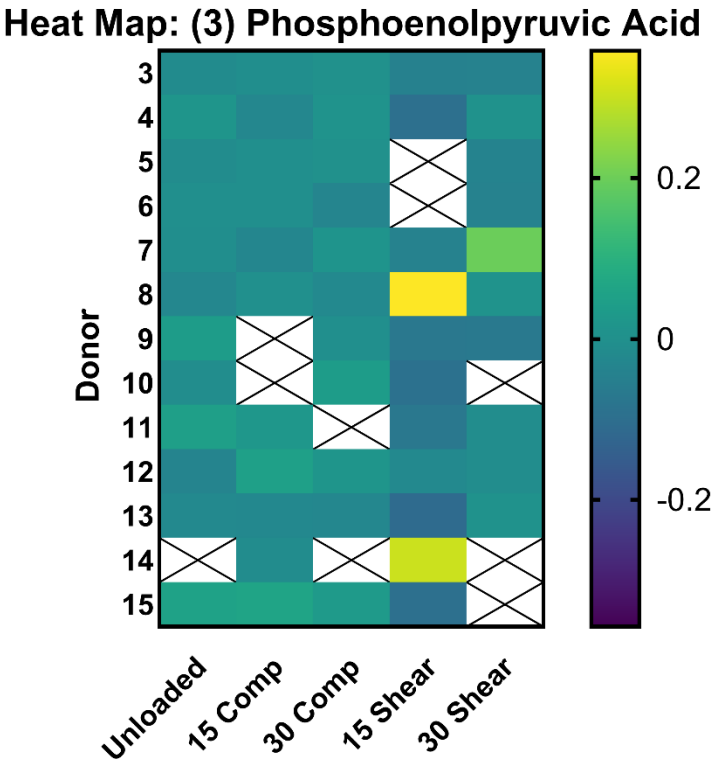
Heat Map: (3) Phosphoenolpyruvic Acid
Donor
3
4
5
6
7
8
9
10
11
12
13
14
15
Unloaded
15 Comp
30 Comp
15 Shear
30 Shear
0.2
0
-0.2

495

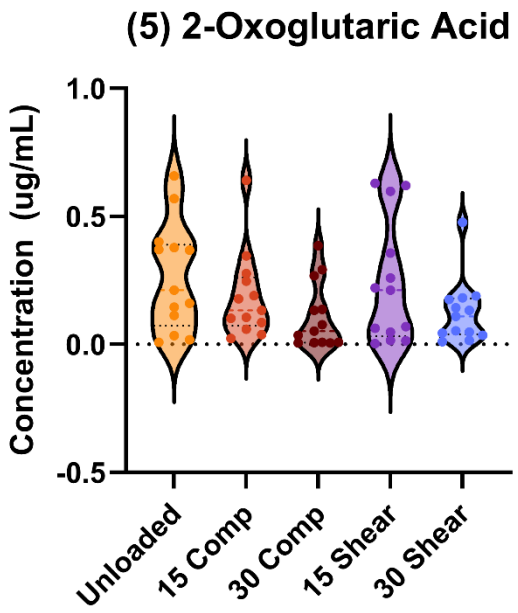
(5) 2-Oxoglutaric Acid
Concentration (ug/mL)
1.0
0.5
0.0
-0.5
Unloaded
15 Comp
30 Comp
15 Shear
30 Shear

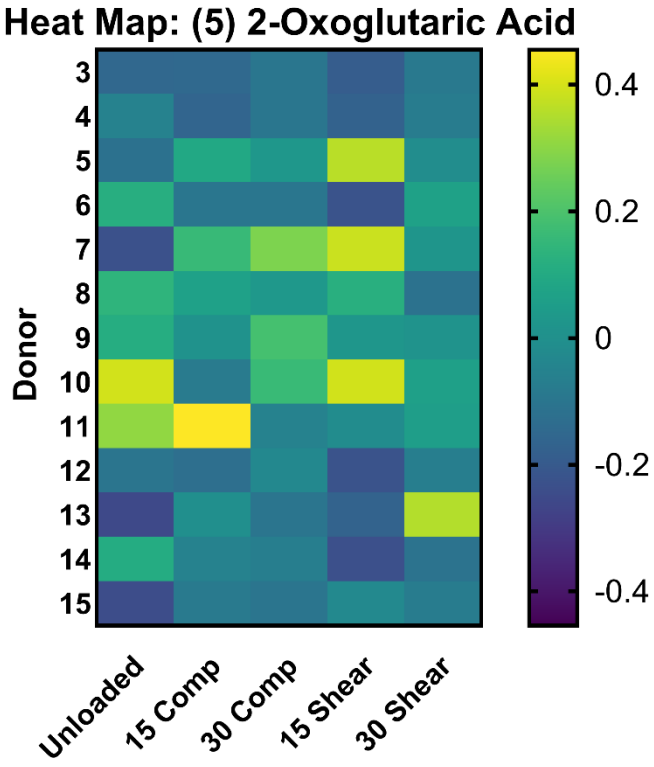
Heat Map: (5) 2-Oxoglutaric Acid
Donor
3
4
5
6
7
8
9
10
11
12
13
14
15
Unloaded
15 Comp
30 Comp
15 Shear
30 Shear
0.4
0.2
0
-0.2
-0.4

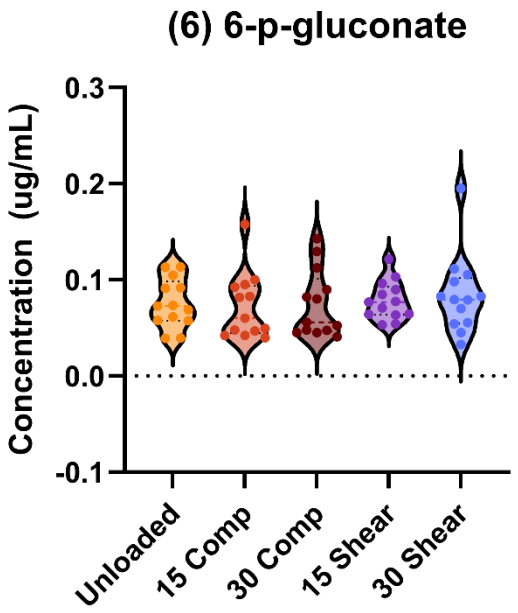
(6) 6-p-gluconate
Concentration (ug/mL)
0.3
0.2
0.1
0.0
-0.1
Unloaded
15 Comp
30 Comp
15 Shear
30 Shear

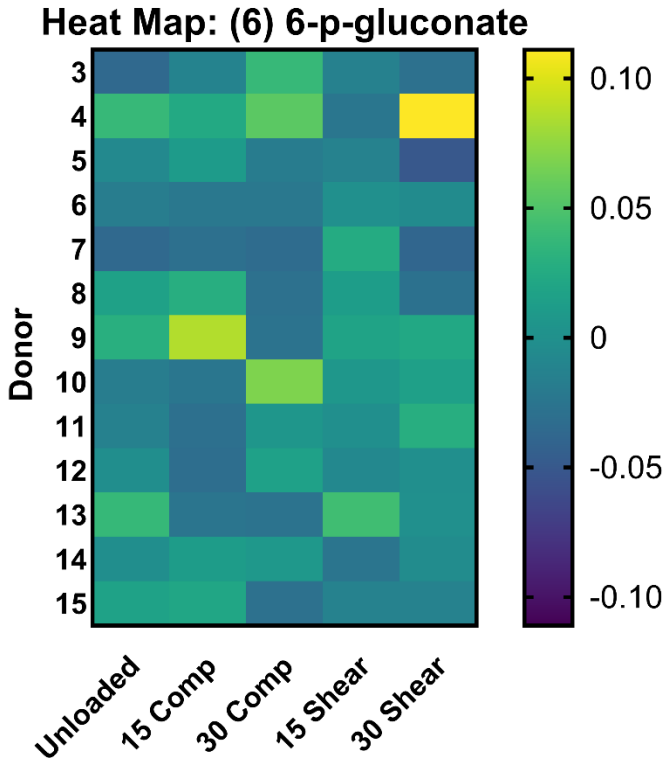
Heat Map: (6) 6-p-gluconate
Donor
3
4
5
6
7
8
9
10
11
12
13
14
15
Unloaded
15 Comp
30 Comp
15 Shear
30 Shear
0.10
0.05
0
-0.05
-0.10

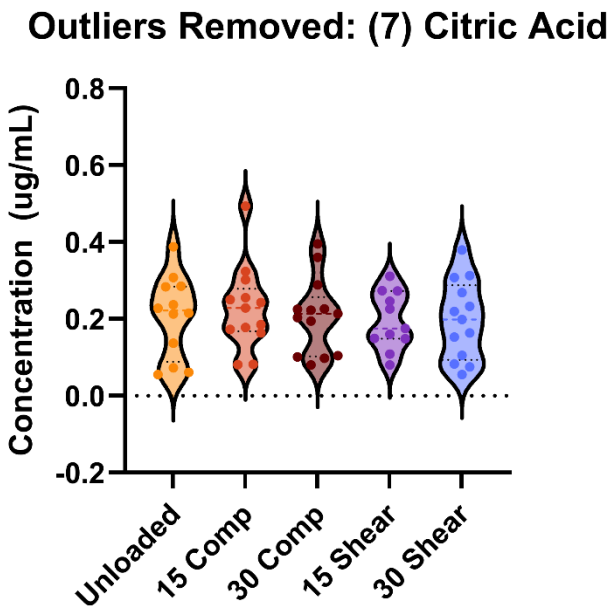
Outliers Removed: (7) Citric Acid
Concentration (ug/mL)
0.8
0.6
0.4
0.2
0.0
-0.2
Unloaded
15 Comp
30 Comp
15 Shear
30 Shear

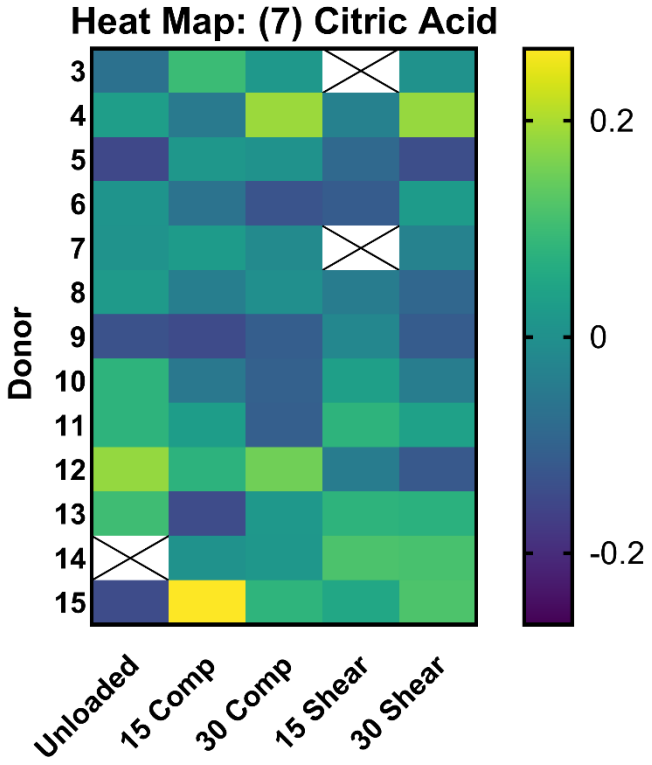
Heat Map: (7) Citric Acid
Donor
3
4
5
6
7
8
9
10
11
12
13
14
15
Unloaded
15 Comp
30 Comp
15 Shear
30 Shear
0.2
0
-0.2

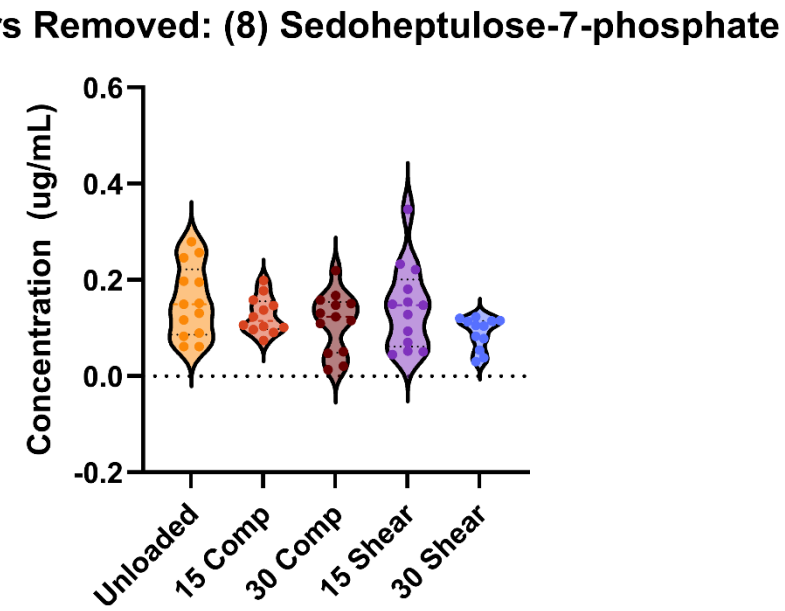
Outiers Removed: (8) Sedoheptulose-7-phosphate
Concentration (ug/mL)
0.6
0.4
0.2
0.0
-0.2
Unloaded
15 Comp
30 Comp
15 Shear
30 Shear

502

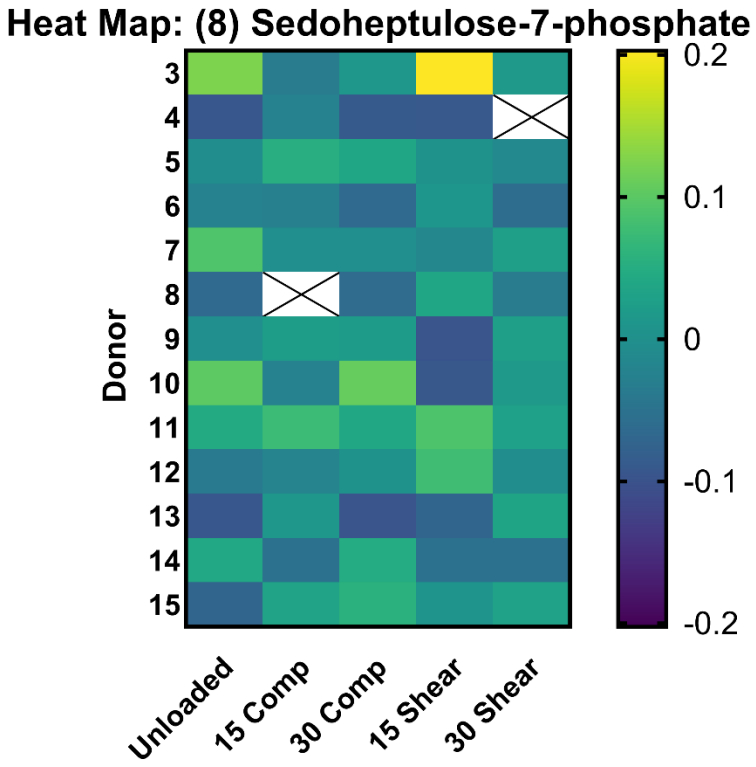
Heat Map: (8) Sedoheptulose-7-phosphate
Donor
3
4
5
6
7
8
9
10
11
12
13
14
15
Unloaded
15 Comp
30 Comp
15 Shear
30 Shear
0.2
0.1
0
-0.1
-0.2

503

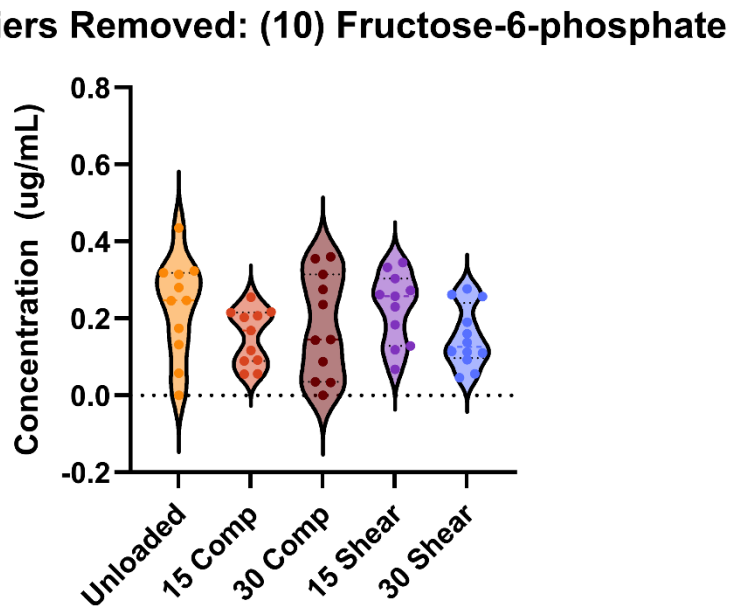
Outliers Removed: (10) Fructose-6-phosphate
Concentration (ug/mL)
0.8
0.6
0.4
0.2
0.0
-0.2
Unloaded
15 Comp
30 Comp
15 Shear
30 Shear

504

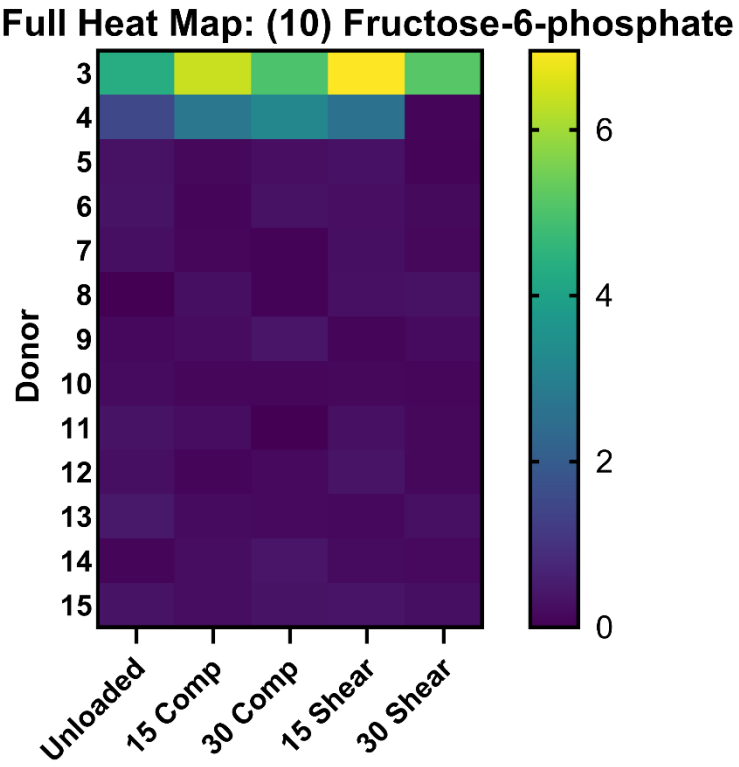
(10) Full Heat Map: (10) Fructose-6-phosphate
Donor
3
4
5
6
7
8
9
10
11
12
13
14
15
Unloaded
15 Comp
30 Comp
15 Shear
30 Shear
6
4
2
0

505

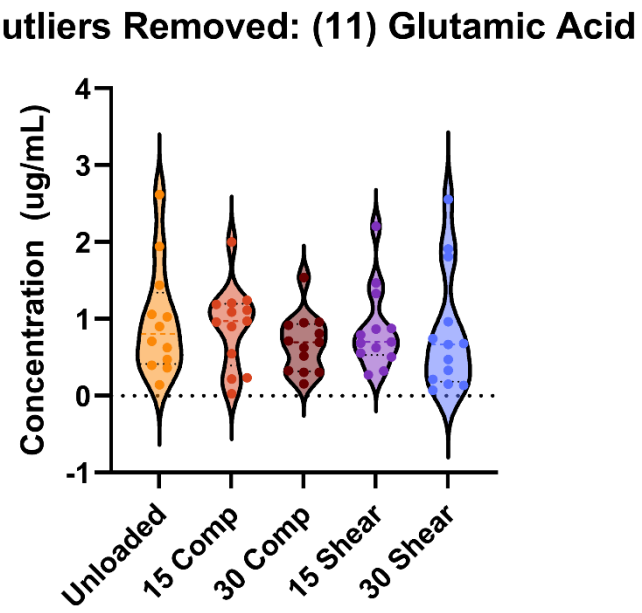
Outliers Removed: (11) Glutamic Acid
Concentration (ug/mL)
4
3
2
1
0
-1
Unloaded
15 Comp
30 Comp
15 Shear
30 Shear

506

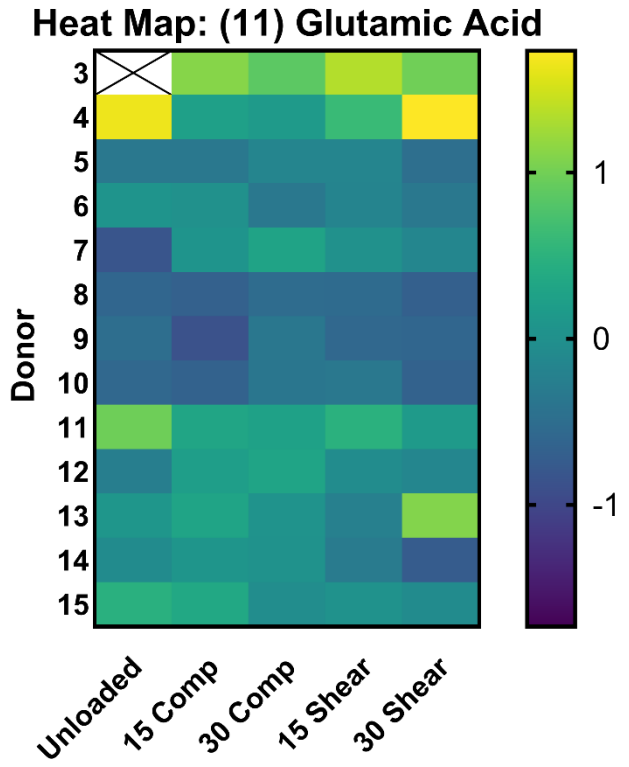
Heat Map: (11) Glutamic Acid
Donor
3
4
5
6
7
8
9
10
11
12
13
14
15
Unloaded
15 Comp
30 Comp
15 Shear
30 Shear
1
0
-1

507

References

Brahmachary PP, Welhaven HD, June RK (2023) Metabolomic Profiling to Understand Chondrocyte Metabolism Methods Mol Biol 2598:141-156 doi:10.1007/978-1-0716-2839-3_11

Chan DD, Cai L, Butz KD, Trippel SB, Nauman EA, Neu CP (2016) In vivo articular cartilage deformation: noninvasive quantification of intratissue strain during joint contact in the human knee Sci Rep 6:19220 doi:10.1038/srep19220

Chery DR et al. (2020) Early changes in cartilage pericellular matrix micromechanobiology portend the onset of post-traumatic osteoarthritis Acta Biomater 111:267-278 doi:10.1016/j.actbio.2020.05.005

Coleman MC, Ramakrishnan PS, Brouillette MJ, Martin JA (2016) Injurious Loading of Articular Cartilage Compromises Chondrocyte Respiratory Function Arthritis Rheumatol 68:662-671 doi:10.1002/art.39460

Doran PM, Morrissey K, Carlson RP (2024) Bioprocess Engineering Principles. 3rd Edition edn. Academic Press,

Ely EV et al. (2025) Chondrocyte-specific knockout of Piezo1 and Piezo2 protects against post-traumatic osteoarthritis structural damage and pain in mice Arthritis Res Ther 27:152 doi:10.1186/s13075-025-03620-w

Haudenschild DR, Chen J, Pang N, Steklov N, Grogan SP, Lotz MK, D'Lima DD (2011) Vimentin contributes to changes in chondrocyte stiffness in osteoarthritis J Orthop Res 29:20-25 doi:10.1002/jor.21198

Huang YF et al. (2023) Lactate-upregulated NADPH-dependent NOX4 expression via HCAR1/PI3K pathway contributes to ROS-induced osteoarthritis chondrocyte damage Redox Biol 67:102867 doi:10.1016/j.redox.2023.102867

Jiang D, Guo J, Liu Y, Li W, Lu D (2023) Glycolysis: an emerging regulator of osteoarthritis Front Immunol 14:1327852 doi:10.3389/fimmu.2023.1327852

Jutila AA, Zignego DL, Schell WJ, June RK (2015) Encapsulation of chondrocytes in high-stiffness agarose microenvironments for in vitro modeling of osteoarthritis mechanotransduction Ann Biomed Eng 43:1132-1144 doi:10.1007/s10439-014-1183-5

Mauck RL, Yuan X, Tuan RS (2006) Chondrogenic differentiation and functional maturation of bovine mesenchymal stem cells in long-term agarose culture Osteoarthritis Cartilage 14:179-189 doi:10.1016/j.joca.2005.09.002

Mosher TJ, Liu Y, Torok CM (2010) Functional cartilage MRI T2 mapping: evaluating the effect of age and training on knee cartilage response to running Osteoarthritis Cartilage 18:358-364 doi:10.1016/j.joca.2009.11.011

Ohashi T, Hagiwara M, Bader DL, Knight MM (2006) Intracellular mechanics and mechanotransduction associated with chondrocyte deformation during pipette aspiration Biorheology 43:201-214

547 Sah RL, Kim YJ, Doong JY, Grodzinsky AJ, Plaas AH, Sandy JD (1989) Biosynthetic
548 response of cartilage explants to dynamic compression J Orthop Res 7:619-636
549 doi:10.1002/jor.1100070502

550 Shodiev DR, Zvyagina VI, Ryabova MN, Marsyanova YA (2024) Succinate-receptor
551 system of bone and cartilage tissue in patients with metabolic phenotype of
552 osteoarthritis BMP-chemistry 27:41-49 doi:10.29296/25877313-2024-09-06

553 Tan C, Li L, Han J, Xu K, Liu X (2022) A new strategy for osteoarthritis therapy: Inhibition
554 of glycolysis Front Pharmacol 13:1057229 doi:10.3389/fphar.2022.1057229

555 Tonge DP, Pearson MJ, Jones SW (2014) The hallmarks of osteoarthritis and the potential
556 to develop personalised disease-modifying pharmacological therapeutics
557 Osteoarthritis Cartilage 22:609-621 doi:10.1016/j.joca.2014.03.004

558 Zhao Z, Li Y, Wang M, Zhao S, Zhao Z, Fang J (2020) Mechanotransduction pathways in
559 the regulation of cartilage chondrocyte homoeostasis J Cell Mol Med 24:5408-
560 5419 doi:10.1111/jcmm.15204

561 Zignego DL, Hilmer JK, June RK (2015) Mechanotransduction in primary human
562 osteoarthritic chondrocytes is mediated by metabolism of energy, lipids, and amino
563 acids J Biomech 48:4253-4261 doi:10.1016/j.jbiomech.2015.10.038

564 Zignego DL, Jutila AA, Gelbke MK, Gannon DM, June RK (2014) The mechanical
565 microenvironment of high concentration agarose for applying deformation to
566 primary chondrocytes J Biomech 47:2143-2148
567 doi:10.1016/j.jbiomech.2013.10.051

568